อนุภาคคาร์บอนระดับนาโนเมตรที่ถูกออกซิไดซ์เพื่อเป็นตัวพายา

นางสาวกิตติมา อมรวชิรบดี

วิทยานิพนธ์นี้เป็นส่วนหนึ่งของการศึกษาตามหลักสูตรปริญญาวิทยาศาสตรดุษฎีบัณฑิต
สาขาวิชาเคมี ภาควิชาเคมี
คณะวิทยาศาสตร์ จุฬาลงกรณ์มหาวิทยาลัย
ปีการศึกษา 2559

OXIDIZED CARBON NANOPARTICLES AS DRUG CARRIERS

Miss Kittima Amornwachirabodee

A Dissertation Submitted in Partial Fulfillment of the Requirements
for the Degree of Doctor of Philosophy Program in Chemistry
Department of Chemistry
Faculty of Science
Chulalongkorn University
Academic Year 2016

Thesis Title	OXIDIZED CARBON NANOPARTICLES AS DRUG CARRIERS
By	Miss Kittima Amornwachirabodee
Field of Study	Chemistry
Thesis Advisor	Professor Supason Wanichwecharungruang, Ph.D.
Thesis Co-Advisor	Prompong Pienpinijtham, Ph.D.

Accepted by the Faculty of Science, Chulalongkorn University in Partial Fulfillment of the Requirements for the Doctoral Degree

.....Dean of the Faculty of Science
(Associate Professor Polkit Sangvanich, Ph.D.)

THESIS COMMITTEE

.....Chairman
(Assistant Professor Varawut Tangpasuthadol, Ph.D.)

.....Thesis Advisor
(Professor Supason Wanichwecharungruang, Ph.D.)

.....Thesis Co-Advisor
(Prompong Pienpinijtham, Ph.D.)

.....Examiner
(Assistant Professor Pattara Thiraphibundet, Ph.D.)

.....Examiner
(Sakulsuk Unarunotai, Ph.D.)

.....Examiner
(Associate Professor Tanapat Palaga, Ph.D.)

.....External Examiner
(Assistant Professor Thitinun Karpkird, Ph.D.)

กิตติมา อมรวชิรบดี : อนุภาคคาร์บอนระดับนาโนเมตรที่ถูกออกซิไดซ์เพื่อเป็นตัวพายา (OXIDIZED CARBON NANOPARTICLES AS DRUG CARRIERS) อ.ที่ปรึกษาวิทยานิพนธ์หลัก: ศ. ดร.ศุภศร วนิชเวชารุ่งเรือง, อ.ที่ปรึกษาวิทยานิพนธ์ร่วม: อ. ดร.พร้อมพงศ์ เพียรพินิจธรรม, 77 หน้า.

อนุภาคออกซิไดซ์คาร์บอนแบล็กขนาดนาโนเมตรได้ถูกเตรียมขึ้นจากกระบวนการออกซิเดชั่นของคาร์บอนแบล็ก ซึ่งอนุภาคที่สังเคราะห์ได้ถูกเรียกว่า oxidized carbon black nanoparticles (OCBs) โดย OCBs ที่เตรียมได้มีลักษณะเป็นอนุภาคทรงกลมขนาด 100-200 นาโนเมตร มีความสามารถในการกระจายตัวในน้ำได้ดี และประกอบด้วยหมู่ฟังก์ชั่นทางเคมีคืออีพ็อกไซด์ คาร์บอกซิลิก และ ไฮดรอกซิลที่ผิวของอนุภาค เมื่อนำOCBsไปทดสอบในเซลล์ พบว่า OCBs ไม่มีความเป็นพิษต่อเซลล์ไลน์มะเร็งเม็ดเลือดขาว(RAW 264.7) ที่ความเข้มข้น 3 ไมโครกรัมต่อไมโครลิตร เซลล์มะเร็งปากมดลูกมนุษย์ (CaSki) ที่ความเข้มข้น 10 ไมโครกรัมต่อไมโครลิตร และเซลล์เคราติโทไซต์ (keratinocyte) ที่ความเข้มข้นสูงถึง 30 ไมโครกรัมต่อไมโครลิตร จากการทดสอบการแทรกผ่านเข้าไปในลิโพโซมซึ่งเป็นแบบจำลองของเซลล์เมมเบรน พบว่า OCBs สามารถแทรกผ่านเข้าไปภายในลิโพโซมได้และยังสามารถช่วยเพิ่มการแทรกผ่านของโปรตีนขนาด 300 กิโลดาลตัน และอนุภาคขนาดไมโคร/นาโนเมตร เข้าไปภายในลิโพโซมได้ดีขึ้น นอกจากนั้นเมื่อทำการทดลองใช้ OCBs ในการนำส่งโปรตีนและอนุภาคขนาดไมโคร/นาโนเมตรเข้าสู่เซลล์พบว่า OCBs สามารถนำส่งสารดังกล่าวเข้าสู่เซลล์ได้โดยไม่ผ่านกระบวนการเอ็นไดไซโตซิส (endocytic pathway) และสามารถนำส่งสารได้ทั้งในไซโทพลาสซึมและนิวเคลียสของเซลล์ ดังนั้น OCBs จึงเป็นตัวนำส่งที่ทำหน้าที่นำส่งสารออกฤทธิ์ที่มีโมเลกุลขนาดใหญ่เข้าสู่เซลล์ได้อย่างมีประสิทธิภาพ

ภาควิชา เคมี	ลายมือชื่อนิสิต .....
สาขาวิชา เคมี	ลายมือชื่อ อ.ที่ปรึกษาหลัก .....
ปีการศึกษา 2559	ลายมือชื่อ อ.ที่ปรึกษาร่วม .....

5572803323 : MAJOR CHEMISTRY

KEYWORDS: CARBON BLACK, OXIDIZED CARBON NANOPARTICLES, DELIVERY SYSTEM, PROTEIN DELIVERY, MEMBRANE LEAK

KITTIMA AMORNWACHIRABODEE: OXIDIZED CARBON NANOPARTICLES AS DRUG CARRIERS. ADVISOR: PROF. SUPASON WANICHWECHARUNGRUANG, Ph.D., CO-ADVISOR: PROMPONG PIENPINIJTHAM, Ph.D., 77 pp.

Oxidized carbon black nanoparticles (OCBs) are successfully synthesized by modify exfoliation/oxidation process from commercially available carbon black. OCBs are 100-200 nm stable water dispersible with spherical shape. The particles contain mainly disordered **π**-**π** conjugation network of carbon atoms, with epoxide, carboxylic, and hydroxyl functionality on the surface. OCBs show no cytotoxicity against macrophage cell line (RAW 264.7), human cervical carcinoma cell line (CaSki) and keratinocyte cells, at the concentration up to 3 μg/mL, 10 μg/mL and 30 μg/mL, respectively. Experiments with cell-sized liposomes indicate that OCBs directly interact with phospholipids and induce membrane leakages. Moreover, OCBs can speed up both of micro sized and nano sized particles to association with phospholipid bilayer membranes and can increase the penetration of micro/nano particles across the membrane of the liposomes. Furthermore, experiments with cells show that OCBs can deliver a 300 kDa protein and micro/nano particles directly into cells, without an involvement of cellular endocytosis. This could be implied that the delivery by OCBs enhance the cellular penetration of bio-macromolecule and micro/nanoparticles.

Department:	Chemistry	Student's Signature	.....
Field of Study:	Chemistry	Advisor's Signature	.....
Academic Year:	2016	Co-Advisor's Signature	.....

ACKNOWLEDGEMENTS

This study was performed at the Department of Chemistry, Faculty of Science, Chulalongkorn University. I am particularly very grateful to the Royal Golden Jubilee Ph.D. Program (PHD/0261/2553), Thailand for financial support during my doctoral study.

I would like to express my sincere gratitude to my supervisor, Professor Supason Wanichwecharungruang of Chulalongkorn University for her active valuable guidance, helpful suggestions and kindly support during my Ph.D. All of achievements during my study would not be possible without her creative mind and her enthusiastic guidance. I also express my specially thank my second supervisor Dr. Prompong Pienpinijtham for his valuable guidance and creative mind.

I would like to grateful acknowledge Associate Professor Tanapat Palaga for his contributions of time, knowledge and experience on the biological parts.

I would like to express my appreciation to my referees, Assistance Professor Varawut Tangpasuthadol, Assistance Professor Pattara Thiraphibundet, Dr. Sakulsuk Unarunotai, Associate Professor Tanapat Palaga and Assistance Professor Thitinun Karpkird for their assistance to complete my thesis.

I am profoundly grateful to Associate Professor Nipan Israsena and Ms. Supaporn Khramchantuk for their good discussion and supported me in the keratinocyte cell and 3-D skin experiments.

I also thank to all members of Professor Supason's laboratory who supported me throughout my Ph.D. Finally, I would like to express my heartfelt appreciation to my family for thoughtful attention and continuous encouragements.

CONTENTS

Page

Page

Page

LIST OF TABLES

Page

LIST OF FIGURES

Page

LIST OF ABBREVIATIONS

Da	Dalton
eV	Electron volt
mL	Milliliter
µL	Microliter
µm	Micrometer
nm	Nanometer
OCNs	Oxidized carbon nanoparticles
OCBs	Oxidized carbon black nanoparticles
PBS	Phosphate buffer solution
ppm	Parts per million
PRPs	Pro-retinal micro and nano-particles
MWCO	Molecular weight cut-off
w/w	Weight by weight

CHAPTER I
INTRODUCTION

Bioactive macromolecules have the prospect of becoming a new treatment strategy for various diseases. The macromolecules such as antisense oligonucleotides, nucleic acid and peptide aptamers, genes, enzymes, proteins and interfering RNAs could react at the specific pathological phenotypes in the cells [1-3]. The major problem of therapeutic efficiency is the way to deliver therapeutic agents into cellular compartments. Cell membranes are highly selective permeability barrier, which means that some molecules can cross the membranes but macromolecules cannot [4]. The most common mechanism of cellular uptake for therapeutic agent is endocytosis, an active transport process in which the compound is trapped within endosomes that can result in degradation of the drug [5]. In order to improve the therapeutic efficiency, many delivery systems for deliver macromolecule into the cell are developed. Recently, micro/nano particles have been used to enhance the efficiency of drug delivery but the penetration of particles through cell membrane are limited by their sizes [6]. The invasion from endosome to the cells by cationic charged nanomaterials [7, 8], viral vectors [9, 10] and cell penetrating peptides [11] have been used as an effective component of the intracellular delivery systems of bioactive macromolecules. However, these process that are also associated with cytotoxicity, limited loading and complicated preparation [12, 13].

Inspired by our previous work, we have explored the fabrication of the OCNs via sonication assisted chemical exfoliation/oxidation [14]. The OCNs are negatively charged carbon oxide nanospheres with outstanding ability to penetrate lipid bilayer membrane and thus can penetrate into cells efficiently. It has been reported that OCNs can help macromolecules to leak from endosomes and thus helps preventing the materials from lysosomal engulfment and digestion [15]. Although OCNs possess excellent properties to be used as drug carriers, the average synthesis yield of OCNs from graphite or graphene is limited to 8%, and the separation process is quite extensive. Therefore, this research will investigate on another approach to prepare materials that can deliver cargo into cell or nuclease without being trapped in endosome/lysosome. Since OCNs is the oxidized carbon nanoparticles, it is possible that oxidation of carbon black particles may give some interesting particles. Here, carbon black which consists of aggregates of spherical particles [16] will be used as a raw material to prepare carbon oxide nanosphreres for deliver bioactive macromolecules and micro/nano particles.

CHAPTER II
THEORY AND LITERATURE REVIEW

2.1 Entry into the cell

Plasma membrane (or cell membrane) of the cell separates intracellular from extracellular compartments. The cell membrane is a complex composite of multiple lipid species and membrane proteins. The exchanges between inside and outside of the cell depend on the properties of membrane and substance. Therefore, the cell membrane are selective barriers. The transport of substances across cell membrane influenced by their size and their solubility in lipids. Small molecules or lipid-soluble substances can penetrate across the phospholipid bilayer membrane (passive transport). In the case of large molecules can transport via endocytosis (active transport) [17].

2.1.1 Endocytic pathway (active transport)

The endocytic pathways occur by multiple mechanisms that can be divided into two categories; phagocytosis and pinocytosis (Figure2.1). The choice of which endocytic pathway is utilized may depend on the substances. The phagocytosis is cellular uptake process that proceeded by specialized cells as macrophage to clear large pathogens. In contrast, pinocytosis occurs in all cells which can divided into four mechanisms; macropinocytosis, clathrin-mediated endocytosis (CME), caveolae-mediated endocytosis, and clathrin- and caveolae-independent endocytosis [5].

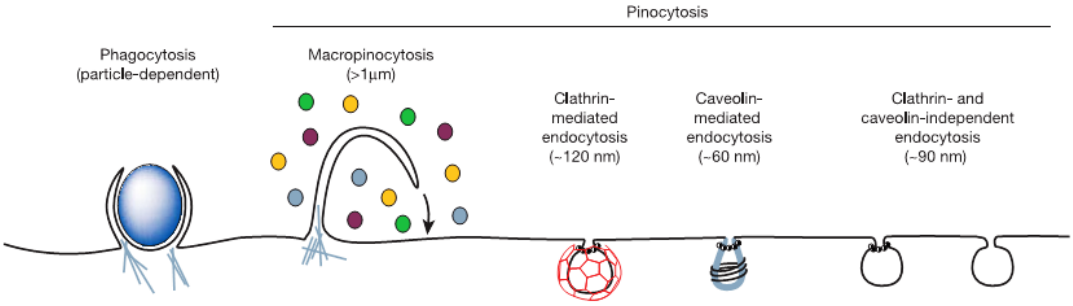

Figure 2.1 Multiple portals of entry into the mammalian cell. The endocytic pathways differ with regard to the size of the endocytic vesicle, the nature of the cargo (ligands, receptors and lipids) and the mechanism of vesicle formation. [5]

Clathrin-dependent and independent routes of endocytosis generate primary endocytic vesicles that subsequently fuse with early endosomes. Early endosomes serve as the major sorting stations where proteins can be sorted into recycling endosomes for recycling back to the cell surface, into a retrogradee pathway mediated by retromer to be sent back to the trans-golgi network (TGN), or into a degradation pathway for eventual targeting to the lysosome (Figure 2.2) [18, 19].

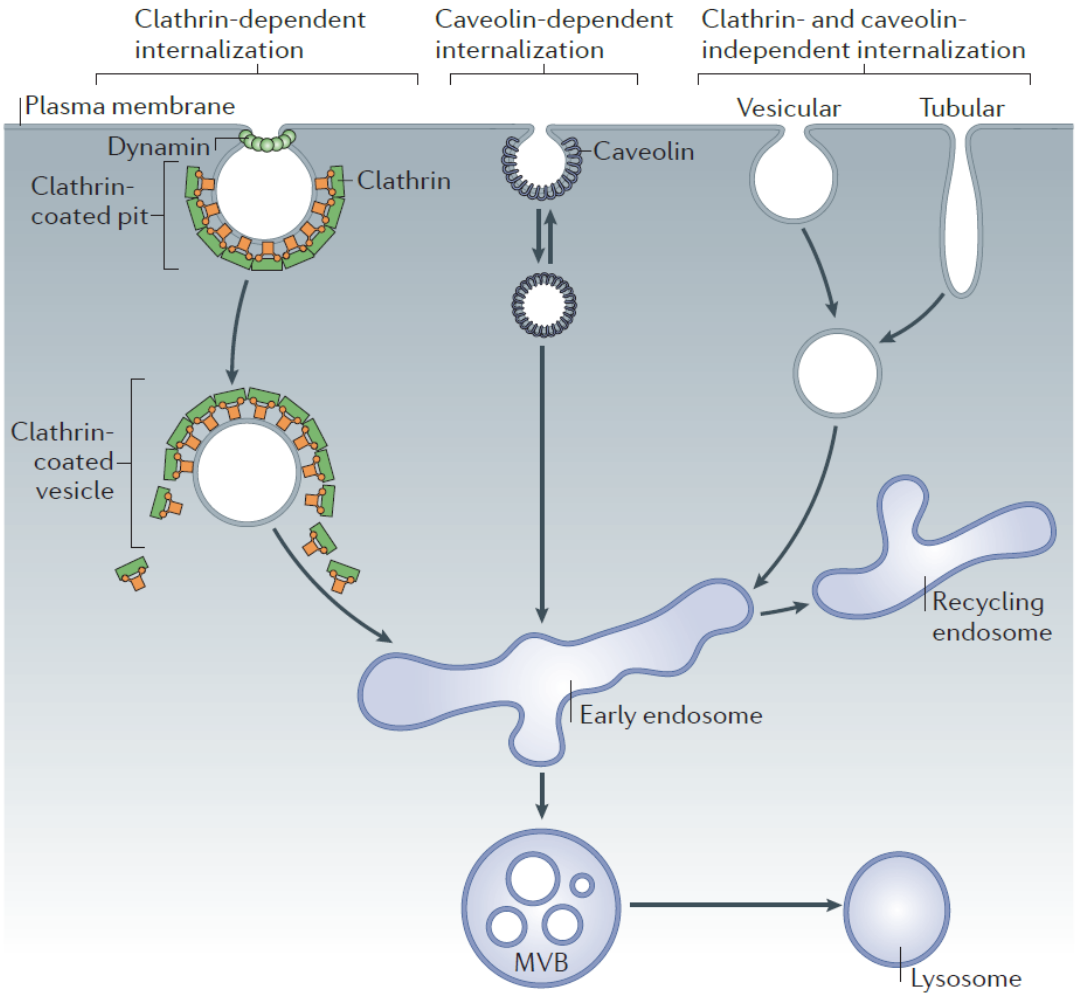

Figure 2.2 Clathrin-dependent and -independent internalization pathways. [18]

2.1.2 Non-endocytic pathway (Passive transport)

Phospholipid bilayer membrane allow for diffusion of lipid soluble molecules (O_2, CO_2, and alcohol). Passive diffusion across a cellular membrane dose not require the use of energy (ATP). Smaller molecules will collide less frequently and therefore diffuse more quickly than larger molecules. While large molecules (proteins or

starches) simply do not diffuse across cell membranes. Thus, the most important parameters that govern transmembrane diffusion are polarity and size of substances [17].

2.2 Delivery of bio-macromolecule into the cell

Bio-macromolecules, including peptides, proteins and siRNAs, possess many desirable therapeutic features that provide unique opportunities to design precision medicine therapeutics to treat human disease. However, due to their size (> 1,000 Da), macromolecules have no bioavailability to cross the cell membrane and enter cells [20, 21]. In order to improve their therapeutic efficiency, transportation of the cargoes that can avoid the endocytic route are required. There are some delivery techniques that use for enhance the penetration of bio-macromolecules across cell membrane [22, 23].

2.2.1 Cell penetrating peptide

Cell penetrating peptide (CPP) are generally composed of 6–30 amino acid residues. The conjugation or stable complex formation of CPPs with molecules of interest facilitates the internalization by target cells, which yields improved bioactivity. CPP has now been widely used to transport a variety of macromolecules into the cells via endocytosis [24-27]. In order to avoid digested by lysosome, the use of cationic molecules can release of cargoes from endosome before the fusion process of the endosome and lysosome, called endosomal escape (Figure 2.3).

The cationic CPPs, such as TAT-PTD, 8R and Penetratin/Antp, have been used over recent years to deliver a multitude of macromolecular into the cell and can cause endosomal escape of molecules (Figure 2.4) [21].[19]

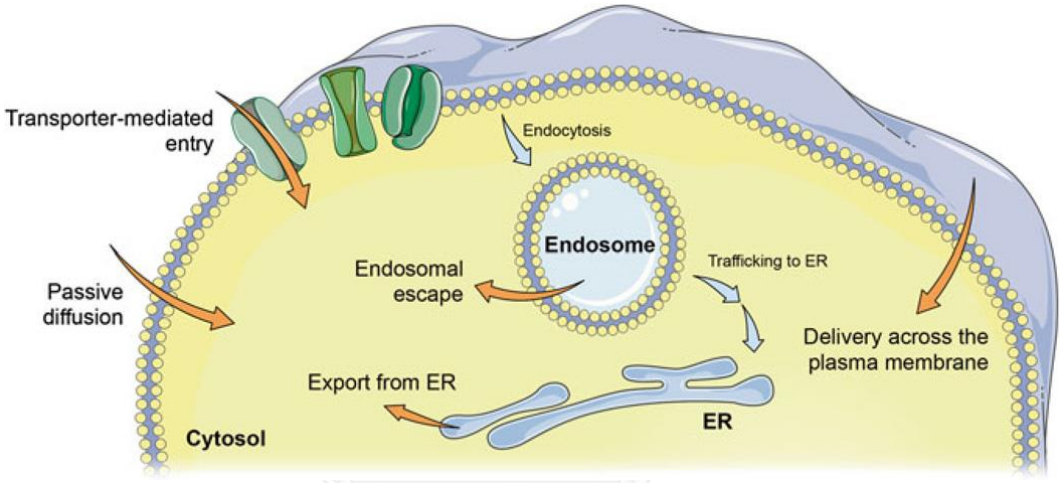

Figure 2.3 The process of endosomal escape. [19]

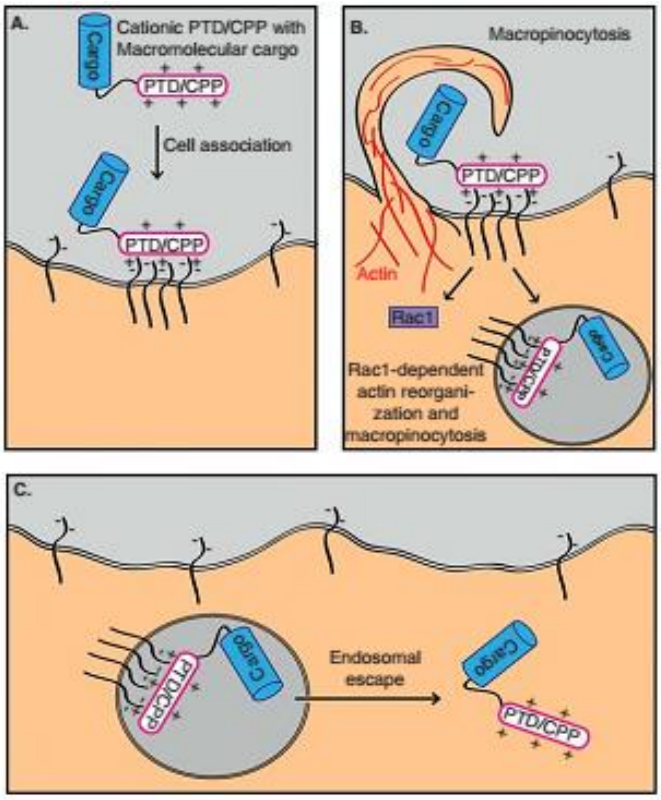

Figure 2.4 Overview of macropinocytotic uptake of cationic PTDs/CPPs. Cationic PTDs/CPPs bind to negatively charged molecules on the cell surface (a) which triggers Rac1-dependent act in reorganization and macropinocytotic uptake (b), and finally the peptides need to escape from endosomes into the cytoplasm (c). [21]

2.2.2 Nanoparticles

Cationic nanoparticles (Diosarg-DOPE NPs) were able to efficiently bind siRNA and plasmid DNA (pDNA) via electrostatic interactions to form stable, nano-sized cationic lipid nanoparticles instead of lamellar vesicles in aqueous solution. The results demonstrated that the self-assembled Diosarg-DOPE NPs could achieve much higher intracellular transport efficiency for siRNA or pDNA than the cationic lipid Diosarg,

indicating that the synergetic effect of different functional lipid components may benefit the development of high efficiency nano-scaled gene carriers. [8]

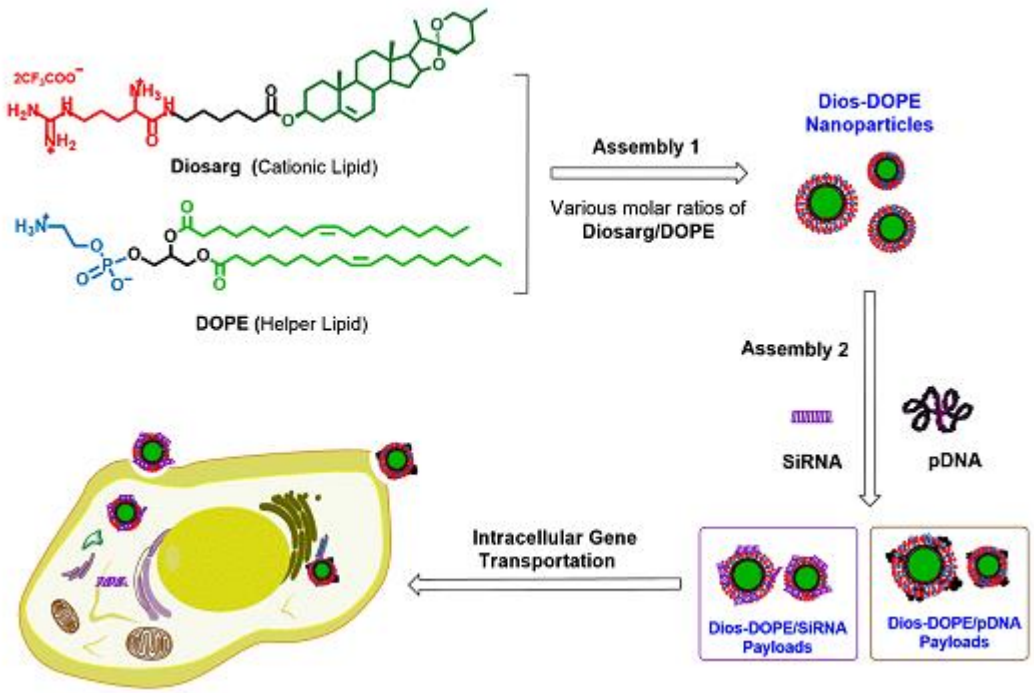

Figure 2.5 Diosarg-1,2-dioleoyl-sn-glycero-3-phosphor-ethanolamine (DOPE) nanoparticles as gene (siRNA and DNA) carriers for intracellular gene transportation. [8]

2.2.3 Viral vector

Drug delivery by viral vector has been intensively studied these days since the viruses possess highly efficient structures and mechanisms to infect in cells with the good targeting with specific types of cells. Therefore, viral vectors can be used as vehicles for gene delivery [9, 10].

Li and co-worker developed denoviral-vector-based intranasal vaccine delivery system by chemically linked TLR-4 agonist, RS09, with DEG-PEI polymer (DP-RS09) or physically mixed TLR-4 with DEG-PEI (DP/RS09) and complexed with adenovirus vaccine. Then cytokine productions on RAW264.7 cells were tested. The results indicated that DEG-PEI could facilitate the intranasal delivery of rAd5 vaccine. Both chemically linked (DP-RS09) and physically mixed RS09 (DP/RS09) could further enhance the mucosal immunity of rAd5 vaccine via TLR-4 pathway [10].

2.3 Carbon Materials as Drug Carrier

Carbon-based nanomaterials, including fullerene, carbon nanotubes, graphene and graphene oxide (Figure 2.6) possess many interesting physical and chemical properties that are potentially useful in biological and biomedical applications [6-8, 28]. Several research aspects involving biomedical applications of various carbon nanomaterials have been reported, including their cytotoxicity, biocompatibility and surface modifications. In addition, it has been shown that using the carbon-based nanomaterials as carriers not only can protect bioactive compounds from enzymatic cleavage but also helps inhibit the binding of various binding proteins to the bioactive compounds [29].

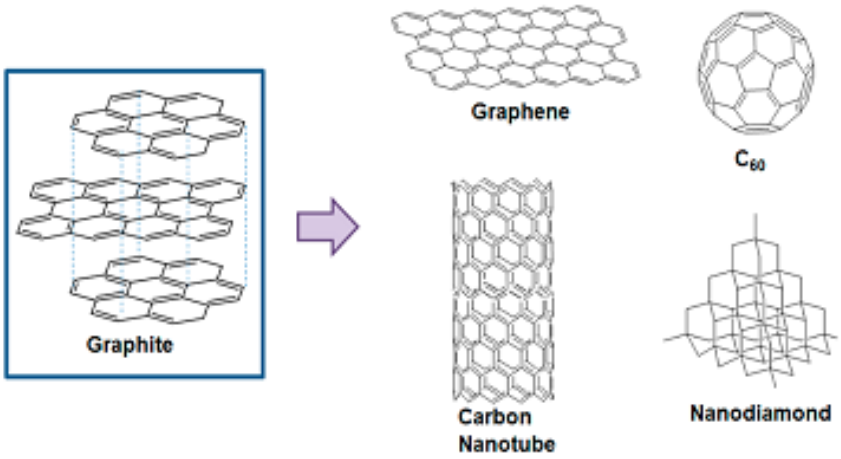

Figure 2.6 Various types of carbon-based nanomaterials. [28]

Wang and co-workers [30] modified graphene oxide for applications in intracellular monitoring and molecular probing such as including DNA sensing, protein assays, and drug delivery. The result showed successful uptake of the aptamer-carboxyfluorescein (FAM)/graphene oxide nanosheet (GO-nS) nanocomplex and cellular target monitoring (Figure 2.7).

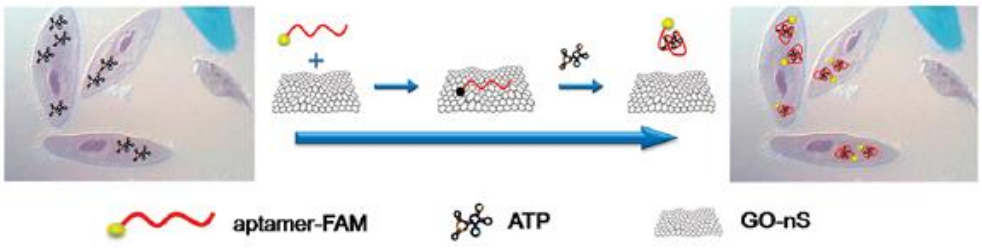

Figure 2.7 Uptaking of aptamer-FAM/GO-nS nanocomplex and cellular target monitoring. [30]

Feng and co-worker [31] prepared graphene oxide (GO) bounded with cationic polymers (polyethyleneimine (PEI)). The positively charged GO-PEI complexes were binded with plasmid DNA (pDNA) for intracellular transfection (Figure 2.8). The results suggest graphene to be a novel gene delivery nano-vector with low cytotoxicity and high transfection efficiency.

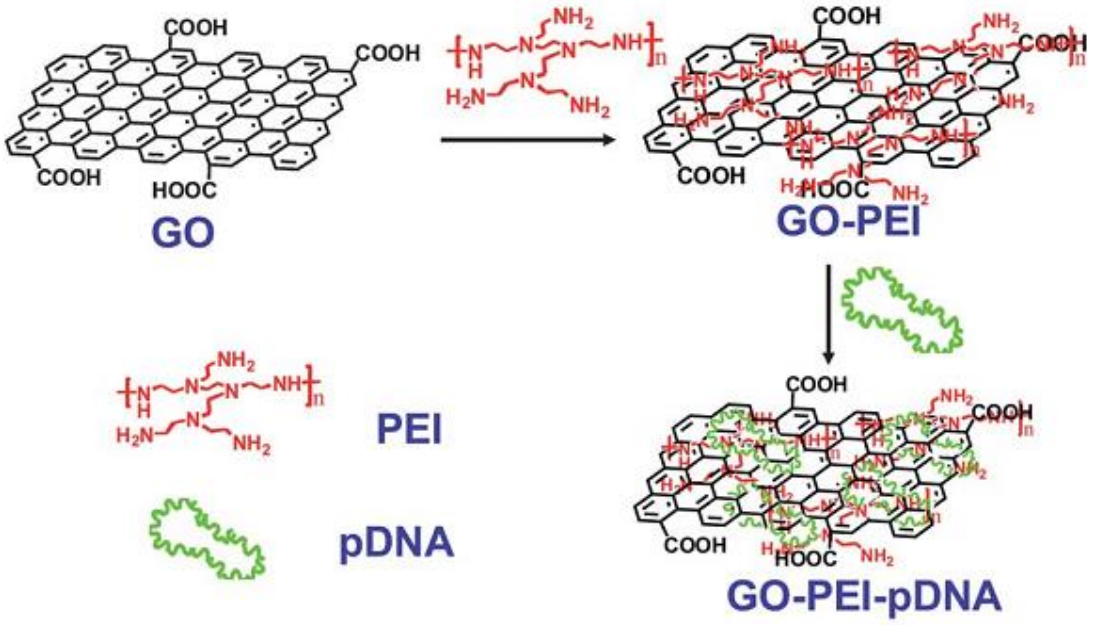

Figure 2.8 Schematic illustration showing the synthesis of GO-PEI-DNA complexes. [31]

Chen and co-worker [32] prepared PEGylated graphene oxide (GO-PEG) and loaded protein onto (GO-PEG) with high payload via noncovalent interactions. GO-PEG could deliver proteins to cytoplasm efficiently, protecting them from enzymatic hydrolysis. The results showed that the proteins ribonuclease A (RNase A) and protein kinase A (PKA) delivered by GO-PEG reserves its biological activity that regulates the cell fate.

Recently, Arayachukait and co-worker have explored the fabrication of the oxidized carbon nanospheres (OCNs) from graphite or graphene nanoplatelets *via* sonication assisted chemical exfoliation/oxidation (Figure 2.9) [14, 15]. The OCNs are negatively charged carbon oxide nanospheres with outstanding ability to penetrate lipid bilayer membrane and thus can penetrate into cells efficiently. It has been reported that OCNs can help macromolecules to leak from endosomes and helps the active materials from lysosomal digestion [15].

Figure 2.9 Synthesis of oxidized carbon nanospheres (OCNs). [14]

2.4 Research objective

Although OCNs possess excellent properties to be used as a carrier to deliver matters into cells but it has some limit such as low yield and complicated in purification processes. In order to overcome these drawbacks, in this thesis, we will prepare the oxidized carbon nanoparticles from commercially available carbon black particles. The products were characterized for their morphology and chemical composition. In addition, the mechanism of the uptake ability will be studied in details using cell-sized liposomes. Furthermore, the cellular delivery of protein, and micro/nanoparticles by oxidized carbon black nanoparticles will be studied.

The aims of this research can be summarized as follow:

1. To synthesize and characterize oxidized carbon nanoparticles from commercially available carbon black

2. To use the obtained oxidized carbon black nanoparticles as carrier for protein and micro/nano particles delivery

3. To track intracellular trafficking of oxidized carbon black nanoparticles, protein and micro/nano particles

4. To evaluate the toxicity of oxidized carbon black nanoparticles on 3-D skin model

CHAPTER III
EXPERIMENTAL

3.1. Materials and chemicals

Carbon black was obtained from Denka Company (Denki Kagaku Kogyo Kabushiki Kaisha, Japan). 5-carboxyfluorescein (fluorescein), coumarin-3-carboxylic acid (coumarin) and 5-carboxytetramethylrhodamine (TAMRA) were purchased from Life Technologies (CA, USA). 1-ethyl-3-(3-dimethylaminopropyl)-carbodiimide (EDCI) and N-hydroxysuccinamide (NHS) were purchased from Acros Organics (Geel, Belgium). Hen egg white lysozyme protein (MW of 300 kDa), mitomycin C, hydrocortisone, bovine serum albumin (BSA), cholesterol and retinaldehyde were purchased from Sigma Aldrich (St. Louis, USA). N-succinylchitosan (MW of ~ 50000 -68000 Da, % DS = 86) was obtained from Welltech Biotechnology Co. Ltd., (Bangkok, Thiland). Dioleoyl L-**α** phosphatidylcholine (DOPC) and L-**α**-phosphatidylcholine (Egg PC) were purchased from Avanti Polar Lipid (Alabama, USA). Macrophage-like cell line (RAW 264.7), human epidermoid cervical carcinoma cell line (CaSki), mouse embryo fibroblast cells line (3T3), keratinocytes and human liver cancer cell line (Hep G2) were purchased from American type culture collection (ATCC). Dulbecco's modified Eagle medium (DMEM), Roswell Park Memorial Institute medium 1640 (RPMI 1640 medium), fetal bovine serum (FBS), sodium pyruvate, N-2-hydroxyethylpiperazine-N'-2-ethanesulfonic acid (HEPES), penicillin streptomycin sulphate and L-glutamine were purchased from Hyclone

Laboratory, Inc., (Logan, USA). Lysotracker and early endosome fluorescent dye were purchased from Invitrogen (Paisley, USA). Chamber slide system 8-wells was purchased from Lab-Tek II Chambered Cover glass (NY, USA). Dialysis cellulose membrane (MWCO = 12-14 kDa) was purchased from Sigma Aldrich (St. Louis, USA). EpiSkin™ was purchased from EpiSkin Research Institute (Lyon, France). All other chemicals were reagent grade.

3.2. Preparation and characterization of oxidized carbon black nanoparticles (OCBs)

The oxidized carbon black nanoparticles (OCBs) were prepared by using modified exfoliation/oxidation process [14]. The condition of oxidation was optimized by varying the ratios between carbon black and oxidizing agent (Table 3.1). Firstly, carbon black was mixed with 1.0 g of sodium nitrate and the mixture was dispersed in 50 mL of 18 M sulfuric acid. After that the mixture was sonicated at 40 kHz at room temperature for 1 h. Next, potassium permanganate ($KMnO_4$) was slowly added into the mixture with stirring for 90 min. Then 100 mL of distilled water was added and the mixture was heat up to 90°C and stirred for another 30 min. After that, 300 mL of distilled water was then added into the mixture and stirring was continued for another 10 min at room temperature. Subsequently, excess $KMnO_4$ was eliminated by adding 5% (w/v) hydrogen peroxide (50 mL) and stirring at room temperature for 30 min. Finally, the obtained product was washed with water under high speed centrifugation

at 37,600 g (20,000 rpm, for 20 min, 3 times), and the pellet was collected. The pellet was re-suspended in 10 mL water then the suspension was poured into a dialysis bag and dialyzed in water until pH 5.5.

Table 3.1 Various condition for OCBs preparation

Condition	Carbon black (g)	$KMnO_4$ (g)
OCB1	0.1	6.0
OCB2	0.3	6.0
OCB3	0.5	6.0

Morphology and size characterization

The morphology and size of samples were analyzed by scanning electron microscopy (SEM, JEOL JSM-6400, Tokyo, Japan, using an accelerating voltage of 15 kV) and transmission electron microscopy (TEM, JEOL JEM-2100, Tokyo, Japan, using an accelerating voltage of 120 kV in conjunction with selected area electron diffraction). The hydrodynamic size and zeta potential were measured by dynamic light scattering (DLS, Malvern Zetasizer nanoseries model S4700, using a He–Ne laser beam at 632.8 nm and scattering angle of 173°).

Chemical functional groups characterization

The elemental composition and surface functional groups of OCBs were analyzed by elemental analysis (EA, combustion through the PE2400 Series II, Perkin-Elmer, MA, USA), ATR-FTIR (Nicolet 6700, Thermo Scientific, Thermo Fisher Scientific Inc., MA, USA), DXR Raman microscope [(Thermo Scientific, Thermo Fisher Scientific Inc., MA, USA) with a 10X objective and a 5 mW diode laser (λ= 780 nm) excitation source], X-ray photoelectronic spectroscopy (XPS, Kratos RAXIS Ultra DLD instrument, Kratos, Manchester, England instrument using a monochromatic Al KαX-ray source at 1486.6 eV and operated at 150 W, 15 kV and 10 mA, of which high resolution spectra (C1s and O1s) were acquired using a pass energy of 20 and 0.1 eV energy steps and all binding energies were referenced to the hydrocarbon C1s peak at 285 eV), and UV-visible absorption analysis (Shimadzu Corp., Kyoto, Japan).

3.3. Preparation of fluorescence dye labelling OCBs

In this study, the penetration property of OCBs into liposome and living cells were investigated. To observe their behavior, OCBs were labelled with fluorescence dyes before experiment. The fluorescein-labelled OCBs (flu-OCBs), coumarin-labelled OCBs (cou-OCBs) and TAMRA-labelled OCBs (TAMRA-OCBs) were prepared by the following procedure. Firstly, 2.2 mg of EDCI in water (1.0 mL) was slowly added into aqueous suspension of the oxidized carbon black (400 ppm, 5.0 mL) at 0 ^{o}C, under N_2 atmosphere. The reaction was further stirred for 30 min. After that, 1.3 mg of NHS in

water (1.0 mL) was dropped into the reaction, followed by an addition of fluorescence dye solution in DMF (2000 ppm, 0.5 mL). The reaction was stirred for overnight. All products were purified by dialysis bag.

3.4. Penetration of OCBs into liposome

Cell-sized liposome was prepared by lipid film hydration method. Firstly, 200 µL of 2 mM DOPC in chloroform was mixed with 120 µL of 10 mM glucose in methanol. Then, the mixture was dried under nitrogen gas to make a thin film and then the film was kept under vacuum for 24 h. After that, 2.0 mL of water was slowly added and the solution was kept at 37 °C for 3 h in order to hydrate the film and allow the formation of cell-sized liposomes. The liposomes in the suspension of water was dropped onto the glass slide with a silicon chamber then observed under using confocal laser fluorescence microscope (CLFM) (Nikon Digital Eclipse C1-Si, equipped with Plan Apochromat VC 100×, BDLaser (MellesGriot, Carlsbad, CA, USA), a Nikon TE2000-U microscope, a 32-channel PMT-spectral-detector and Nikon-EZ-C1 Gold Version 3.80 software) with a diode laser (559 nm). To investigate the penetration of OCBs into liposome, the obtained liposome suspension in water was mixed with flu-OCBs. The final concentrations of liposomes and flu-OCBs were controlled at 0.25 mM and 100 µg/mL, respectively. After mixing, the suspension was instantly dropped onto the glass slide with a silicon chamber and observed under using CLFM with $\lambda_{ex}/\lambda_{em}$ of 488/520 nm. [15]

3.5. Anthocyanin leakage by OCBs

To prepare cell-size liposomes containing anthocyanin, the dried film of DOPC was prepared using the same protocol as normal liposome preparation (see in 3.4). After the film completely dry, 2.0 mL of 1000 μg/mL anthocyanin solution in water was added to hydrate the film instead of pure water and the solution was kept at 37 ^{o}C for 3 h to allow the formation of cell-size liposomes containing anthocyanin inside the vesicle. In order to eliminate excess anthocyanin outside liposomes, the liposome suspension was left to allow sedimentation. Then, certain volume of water above the sediment liposomes was carefully removed, followed by the addition of same volume pure water [15, 33]. We started the experiment by mixed the anthocyanin-filled liposomes suspension with OCBs to give the final concentration of liposomes and OCBs of 0.25 mM and 100 μg/mL, respectively. The liposome suspension was observed using CLFM with $\lambda_{ex}/\lambda_{em}$ of 488/520 nm. Similar observation was carried out on the control anthocyanin-filled liposomes (water was added in place of OCBs suspension). Observation was carried out as a function of incubation time.

3.6. Adsorption of phospholipids on OCBs

The interaction between OCBs and macromolecule was studied. The experiments were carried out by observing changes in sizes and zeta potential of the OCBs after being incubated with different tested materials. OCBs were incubated with various macromolecules (cholesterol, DOPC, Egg PC and BSA) at the ratio of OCB to

tested material is 1:2 (w/w). The mixtures were incubated for 2 h after that non-adsorption molecules were removed by centrifugation (20,000 rpm, 15 min) at 4°C. The precipitate was re-dispersed in MilliQ water then sizes and zeta potential were measured by DLS. The results were analyzed by SPSS program using one-way ANOVA method.

3.7. Cellular trafficking of protein and OCBs

To investigate the delivery ability of OCBs, we used hen egg white lysozyme protein (MW of 300 kDa) as macromolecule model. The lysozyme protein was labelled with fluorescein (flu-lysozyme) by following procedure. Firstly, 4.4 mg of fluorescein in DMF (0.5 mL) was reacted with 5.7 mg of EDCI in water (1.0 mL). The mixed suspension was further stirred at 4 °C for 30 min. After that, 5.7 mg of NHS in water (1.0 mL) was dropped into the reaction, followed by an addition of 25 mg of lysozyme protein in water (1.0 mL). The reaction was stirred at 4 °C for overnight. Then the products were purified at 4 °C by dialysis bag.

Cellular trafficking of lysozyme protein mixed OCBs was monitored with CaSki cells. CaSki cells were seeded in 8-well chamber at a density of 2×10^6 cells per well, then 50 µl of early endosome fluorescent dye reagent were added and the mixture was incubated overnight at 37 °C in humidified atmosphere (5% CO_2) after that, 50 µL of lysotracker deep red (in anhydrous DMSO) were added (final concentration of lysotracker was 200 nM) and the mixture was incubated for another 2 h at 37 °C. Then,

25 µL of sample (flu-lysozyme mixed with cou-OCBs, at the same concentrations of lysozyme protein and OCBs of 100 ppm) was added directly to cells in each well (to give the final concentration of the lysozyme protein and OCBs in the cell suspension of 10 ppm). After that the live-cells were immediately monitored under CLSM in every 15 min for 4 h. CLSM used was FV10i-LIV (Olympus, Tokyo, Japan) with universal Plan Super Apochomat 60× phase contrast water immersion objective (Lens). Excitation was carried out at 405, 473, 559 and 635 nm (MellesGriot Laser, Carlsbad, CA, USA) and emission was monitored at 450, 520, 584 and 668 nm for cou-OCBs, flu-lysozyme, early endosome specific RFP dye and lysosome specific deep red dye, respectively, using two PMTs that automatically optimized for the detection bandwidth of the four fluorophores. Data were processed with FLUOVIEW 3.0 software.

3.8. Cytotoxicity of OCBs in cell lines

Cytotoxicity OCBs was acquired by MTT assay using RAW 264.7 and CaSki cells. RAW 264.7 cell was maintained in DMEM supplemented with 10% (v/v) FBS, 1% (w/v) sodium pyruvate, 1% (w/v) HEPES, 100 U/mL penicillin and 0.4 mg/mL streptomycin sulphate. CaSki cell was maintained in RPMI 1640 medium with 2.05 mM L-Glutamine. All of the cells were incubated at 37 °C for 24 h in humidified atmosphere (5% CO_2) before experiment. Then, the cells were seeded into a 96 well plates at density of 1×10^4 cells in culture medium. After removal of the culture medium, cells were incubated with OCBs at concentrations of 0.1-100 mg/L in culture media, for 48 h. After

incubation, 10 μL of PBS containing 1 mg/mL MTT solution was added to each well and the plates were incubated for 4 h at 37 °C. After that culture media was removed from the wells and isopropanol (200 μL/well) was added to dissolve formazan crystals. Plates were spin at 4839.77 g for 10 min, then 50 μL of the supernatant was collected and subjected to absorbance measurement at 540 nm by microplate reader (Biochrom Anthos 2010, Biochrom Ltd., Cambridge, UK). All samples were tested in triplicate. Cell viability was calculated using the equation below (Equation 1).

$$\text{Cell viability (\%)} = \frac{\text{ODsample-ODblank}}{\text{ODcontrol-ODblank}} \times 100 \qquad \text{(Eq.1)}$$

3.9. Cellular uptake of OCBs and protein

Firstly, the cellular uptake of OCBs was investigated. In this experiment, TAMRA-labeled OCBs was used to follow the location of OCBs inside the cells. RAW 264.7 at a density of 2×10^6 cells per well were seeded in 6-well plates on cover slips and incubated at 37 °C for 24 h. The cells were incubated with (i) PBS as negative control and (ii) TAMRA-labeled OCBs at the final concentration of 10 ppm. The plate was left for 4 h at 37 °C in a humidified atmosphere (5% CO_2). Cells were washed and replaced with fresh PBS of pH 7.4 three times, and then the cells were fixed by adding 1.0 mL of 4% paraformaldehyde and kept at room temperature for 15 min before being washed with PBS, then the cells were stained nuclei by incubated with 50 μL of 0.01 mg/mL DAPI solution for 10 min and washed with PBS before being subjected to CLFM analysis. Cells were also subjected to CLFM analysis without DAPI incubation. Uptakes

of OCBs into CaSki was carried out similarly but with different culture media. RPMI and 10 ppm TAMRA-labeled OCBs were used for CaSki. Fluorescence signals of DAPI and TAMRA were detected at $\lambda_{ex}/\lambda_{em}$ of 405/450 nm and 561/595 nm, respectively.

Next, the cellular uptake of protein in both of presence and absence of OCBs were observed with CaSki cells. First, CaSki cells at a density of 2×10^6 cells per well were seeded in 6-well plates on cover slips and incubated at 37 °C for 24 h in humidified atmosphere (5% CO_2). Then, CaSki cells were incubated with (i) PBS (negative control), (ii) free flu-lysozyme and (iii) flu-lysozyme mixed with OCBs at lysozyme protein final concentration of 10 ppm and OCBs final concentration of 10 ppm. The plate was left for 4 h at 37 °C in a humidified atmosphere (5% CO_2). Cells were washed and replaced with fresh PBS pH 7.4 three times, and then the cells were fixed by adding 1.0 mL of 4% paraformaldehyde and stained nuclei by DAPI. Then, they were subjected to CLFM analysis. Fluorescence signals of DAPI and fluorescein were detected at $\lambda_{ex}/\lambda_{em}$ of 405/450 nm and 488/520 nm, respectively.

3.10. Preparation and characterization of micro/nanoparticles

The retinal-grafted chitosan particles of various sizes were used as model particles to investigate an ability of the OCBs to bring particles into cells. The pro-retinal micro/nanoparticles (PRPs) were prepared by grafting retinal onto *N*-succinylchitosan, using the following protocol [34]. Firstly, retinaldehyde (30 mg in 2 ml of ethanol) was added drop-wise into aqueous N-SC particle suspension (100 mg in

50 ml of deionized water) under ultrasonic, no light, at 5°C and nitrogen condition. The mixture was continuously ultra-sonicated (40 KHz) for 4 h. Then the obtained PRPs were separated into different sizes by step-wise centrifugation (Table 3.2). Firstly, the mixture was centrifuged at 4,700 g (5,000 rpm, 10 min) to remove impurity in the precipitate. The supernatant was then centrifuged at 7,520 g (8,000 rpm, 15 min). The precipitate was re-dispersed with distilled water. This fraction is called PRP1. Then the supernatant was centrifuged at 15,040 g (16,000 rpm, 15 min). The precipitate was re-dispersed with distilled water to obtain PRP2. The supernatant was centrifuged at 37,600 g (20,000 rpm, 15 min). Finally, the precipitate was re-dispersed with distilled water to obtain PRP3. Then, morphology and size of the obtained products were investigated by SEM and DLS.

Table 3.2 Separation of PRPs by step-wise centrifugation

Rotation speed (RCF)	Time (min)	Precipitate
4700 g	10	Impurity
7,520 g	15	PRP1
15,040 g	15	PRP2
37,600 g	15	PRP3

3.11. Penetration of micro/nano particles into cell-sized liposomes

Cell-sized liposomes were prepared by same method as previous experiment (see in 3.4). Two conditions of PRPs penetration were investigated in this experiment. First in the absence of OCBs, the obtained liposomes suspension in water were mixed with PRP1, PRP2 and PRP3 (at final concentrations of liposomes and PRPs were controlled at 0.25 mM and 100 μg/mL, respectively). Second in the presence of OCBs, the obtained liposomes suspension in water were incubated with the mixture of OCBs and PRPs (ratio of OCBs: PRPs as 1:4) at final concentrations of liposomes and OCBs/PRPs mixture were controlled were 0.25 mM and 100 μg/mL, respectively. After mixing, the suspension was dropped onto the glass slide with a silicon chamber. Then the liposomes in the suspension were observed under using CLFM with $\lambda_{ex}/\lambda_{em}$ of 488/520 nm.

3.12. Cytotoxicity of OCBs and PRPs in keratinocyte

Preparation of condition medium for culturing keratinocyte cells

3T3 cells were cultured in DMEM with 10% (v/v) FBS, 1% (w/v) L-glutamine, 1% (w/v) Penicillin-Streptomycin. After cells completely growth, treated the cells with 10μg / mL mitomycin C in DMEM without serum for 2 h at 37°C, 5% CO_2. Remove the mitomycin C-containing DMEM and wash twice with PBS, added 10 mL of DMEM/F12 medium with 10% (v/v) FBS, 2.5 μg/mL $NaHCO_3$, 0.5 μg/mL hydrocortisone, 1% L-glutamine and 1% Penicillin-Streptomycin. The cells were cultured at 37°C, 5% CO_2 for

24 h, the culture medium were collected and centrifuged at 1000 rpm for 5 min twice. Then growth factor (5 mg/mL human insulin, 20 ng/mL EGF) were added into supernatant for use as keratinocyte culture medium.

Preparation of feeder cells

3T3 cells were cultured in DMEM with 10% (v/v) FBS, 1% (w/v) L-glutamine and 1% (w/v) Penicillin-Streptomycin. After the cells completely growth, they were treated with 10μg/mL mitomycin C in DMEM without serum at 37°C, 5% CO_2 for 2 h. After cells completely growth, the cells were treated with 10μg / mL mitomycin C in DMEM without serum at 37°C, 5% CO_2 for 2 h. Then, 3T3 cells were trypsinized using 0.25% trypsin/EDTA solution at 37°C, 5% CO_2 for 2 min and then DMEM-High glucose, 10% (v/v) FBS, (w/v) L-glutamine and 1% (w/v) Penicillin-Streptomycin were added to stop reaction, spin down for 5 min at 1000 rpm. Discard supernatant carefully and re-suspend in 1.0 mL of DMEM medium, incubated at 37°C, 5% CO_2 for 24 h to obtain feeder cells.

Preparation of keratinocyte cells

Keratinocytes were grown in the presence of feeder cells in DMEM/F12 medium, 10% (v/v) FBS, 2.5 μg/mL $NaHCO_3$, 0.5 μg/mL hydrocortisone, 5 mg/ml human insulin, 20 ng/mL EGF, 1% (w/v) L-glutamine and 1% (w/v) Penicillin-Streptomycin at 37°C, 5% CO_2 for 10-14 days. Then, the keratinocytes were trypsinized using 0.25% trypsin/EDTA solution and used in experiments.

For cytotoxicity test, keratinocytes were seeded into a 96 well plates coated with 10ug/ml collagen type I at density of 1×10^4 cells/well in condition medium at 37°C, 5% CO_2 for 24 h. After removal of the condition medium, cells were incubated with OCBs at concentrations of 0.1-30.0 mg/L in condition medium, for 48 h. After incubation, 10 μL of PBS containing 1 mg/mL MTT solution was added to each well and the plates were incubated for 4 h at 37 °C. After that the medium was removed from the wells and isopropanol (200 μL/well) was added to dissolve formazan crystals. Then subjected to absorbance measurement at 540 nm by microplate reader (Varioskan™ LUX, Thermo Fisher Scientific Inc., MA, USA). All conditions were tested in triplicate. Cell viability was calculated using the equation 3.1

3.13. Cellular uptake and OCBs delivery of micro/nano particles into keratinocytes

Keratinocytes were seeded into a 24 well plates on collagen type I coated cover slips at density of 1×10^5 cells/well in condition medium at 37°C, 5% CO_2 for 24 h. First, we investigated cellular uptake of micro/nano particles in the absence of OCBs, PRP particles (PRP1, PRP2 and PRP3) were added to cells at the final concentration of 2.0 ppm. Second, cellular uptake in the presence of OCBs were observed by treated keratinocytes with PRPs and OCBs mixtures, final concentration of PRPs and OCBs were 2.0 and 30.0 ppm, respectively. Then all of the test plates were left at 37°C, 5% CO_2 for 24 h. The cells were washed and replaced with fresh PBS of pH 7.4 three times, and then the cells were fixed with 4% paraformaldehyde and stained nuclei with DAPI.

After that, all samples were observed under fluorescence microscope (Zeiss Observer Z1, Carl Zeiss Microscopy Ltd., Cambridge, UK.).

3.14. Cellular uptake and OCBs delivery of micro/nano particles into human liver cancer cells (Hep G2)

Hep G2 were maintained in RPMI 1640 medium with 2.05 mM L-Glutamine. All of the cells were incubated at 37 °C, 5% CO_2 for 24 h. After that, Hep G2 were seeded 8-well chamber at a density of 5×10^4 cells/well then 50 µl of early endosome fluorescent dye reagent was added and the mixture was incubated overnight at 37°C, 5% CO_2. Then the test samples (i) PRP2 (final concentration of 2.0 ppm) and (ii) PRP2 plus OCBs (final concentration of PRPs and OCBs as 2.0 and 30.0 ppm, respectively) were added into each well. The plates were incubated at 37 °C, 5% CO_2 for 30 and 60 min. At 30 min before finishing incubation, 50 µL of lysotracker deep red (in anhydrous DMSO) were added (final concentration of lysotracker was 200 nM). Then the cells were fixed with 4% paraformaldehyde and stained nuclei with DAPI. After that, all samples were observed under fluorescence microscope analysis before being monitored under CLSM (FV3000, Olympus, Tokyo, Japan). Excitations were carried out at 405 and 650 nm and emissions were monitored at 462, 618, 520 and 700 nm for DAPI, PRPs, early endosome specific RFP dye and lysosome specific deep red dye, respectively. Data were processed with FV3000-SW software.

3.15. Irritation test of OCBs and PRPs

EpiSkin™ was transferred into 1 mL fresh medium and incubated at 37 °C, 5% CO_2 for 24 h. After that 16 µL of the test substances (OCBs 30 ppm, PRP2 2.0 ppm and PRP2 2.0 ppm plus OCBs 30 ppm) were applied on tissue then all tissue were covered by nylon mesh and incubated at room temperature for 42 min. For each sample, duplicate independent experiments were performed. Exposure to test substances were followed by rising with PBS and mechanically dried. After that, the EpiSkins were transferred to fresh medium and incubated at 37 °C, 5% CO_2 for 42 h, then the cell viability was measured by MTT assay. Sodium dodecyl sulphate (SDS) and PBS were used as positive and negative control, respectively. For each treated tissue, the cell viability is expressed as percentage of the mean negative control tissue. The mean relative tissue cell viability above 50% predicts a non-irritancy potential of test substance [35].

CHAPTER IV
RESULTS AND DISCUSSION

4.1. Preparation and morphology characterization of oxidized carbon black (OCBs)

Commercially available carbon black (CB) was oxidized by an exfoliation/oxidation process of CB with some modification, as detail in chapter III [14]. We experimented with various ratios of carbon black to the oxidizing agent $KMnO_4$, including 0.1:6 g/g (OCB1), 0.3:6 g/g (OCB2) and 0.5:6 g/g (OCB3). In the oxidation condition for OCB1, we obtained a clear solution, implying that too much oxidizing agent (CB: $KMnO_4$ of 0.1: 6) could completely decompose all the carbon black into CO_2 (observed as bubble during reaction). At lower amounts of $KMnO_4$ (OCB2 and OCB3), the homogeneous black suspensions with no precipitation were obtained (Figure 4.1). It should be noted that the commercially available carbon black particles do not disperse in water due to their hydrophobic surface (Figure4.1). The investigation with SEM and TEM indicate that the commercially available carbon black particles are actually aggregates of many spherical particles (Figure 4.2a).

It is very likely that van der Waal's forces or covalent bonds exist between adjacent carbon black nanoparticles in the aggregates. This information agrees with a previous report[36, 37]. The SEM and TEM images of OCB2 (Figure 4.2b) and OCB3 (Figure 4.2c) reveal that the aggregated CB particles (starting material) can be broken

into smaller aggregates by our oxidization process. The different particle size of OCBs caused by amount of oxidizing agents. As mention above, the use of small amount of $KMnO_4$ (ratio of CB: $KMnO_4$ of 0.5:6) lead to the soft explosion of agglomerated carbon black thus non-homogeneous and big size of OCBs were observed. When the ratio of CB: $KMnO_4$ was adjusted into 0.3:6, the increasing of oxidizing agent lead to the strong explosion of agglomerated carbon black then the homogeneous and small OCBs were obtained. In this oxidization condition some of carbon blacks were decomposed into carbon dioxide gas due to the over explosion. Moreover, the increasing of ratio of CB: $KMnO_4$ to 0.1:6 lead to completely explode of all carbon black into carbon dioxide gas. In summary, we successfully obtained oxidized carbon black nanoparticles that dispersed well in water at the ratio of CB: $KMnO_4$ of 0.3: 6.In summary, we successfully obtained oxidized carbon black nanoparticles that dispersed well in water at the ratio of CB: $KMnO_4$ of 0.3: 6.

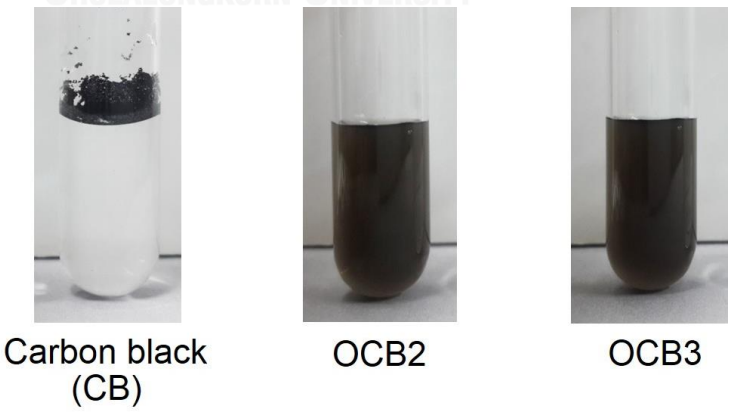

Figure 4.1 Water suspensions of carbon black (CB), oxidized carbon black (OCB2 and OCB3).

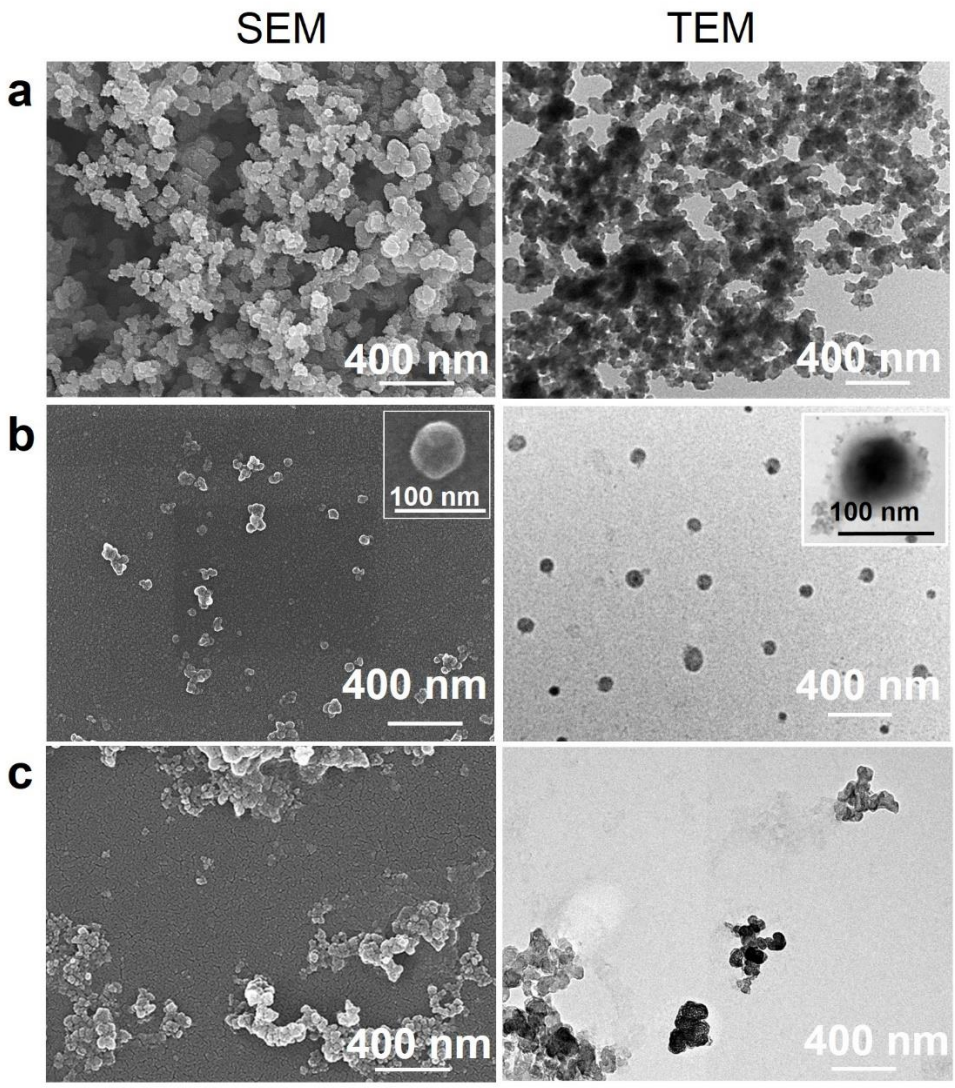

Figure 4.2 Morphology characterization of starting carbon black (CBs) and oxidized carbon black (OCBs). SEM (left) and TEM (right) images of the CBs (a), OCB2 (b) and OCB3 (c).

Table 4.1 shows the particle sizes from SEM, TEM and DLS, we found that the different amounts of $KMnO_4$ gave different sizes of OCBs. Hydrodynamic size and images size (deduced from TEM/SEM images) of OCB2 were smaller than OCB3. Zeta potentials in water of OCB2 and OCB3 were -33.1 ± 1.05 and -34 ± 1.5 mV, respectively. The negatively charged surface (more than -30mV) of both particles well with their

good stability in water [38]. We observed the hydrodynamic size after sonication in a period of time from 0-300 min (Figure 4.3). From the result, we could not be found aggregation or the change in size of OCBs. The polydispersity index (PDI) value of OCB2 (PDI ≈ 0.18) was lower than that of OCB3 (PDI ≈ 0.33). The PDI value of OCB2 was less than 0.2, implying high monodisperse OCBs. According to this results, higher amount of $KMnO_4$ (OCB2 vs OCB3) result in smaller particles with narrower size distribution. Therefore, the best condition for preparation of homogenous dispersion oxidized carbon black nanoparticles was OCB2 (CB: $KMnO_4$ of 0.3: 6). Thus, the OCB2 was used in the rest of the experiments. The synthesis yield of OCB2 was 18% regarding the weight of the starting CB.

Table 4.1 Morphology and size of the oxidized carbon black nanoparticles (OCBs) prepared under different oxidation conditions.

Sample	Weight ratios of CB:$KMnO_4$	SEM size[a] (nm)	TEM size[a] (nm)	DLS		
				Hydrodynamic size (nm)	PDI	Zeta potential (mV)
OCB1	0.1:6.0	-	-	-	-	-
OCB2	0.3:6.0	129 ± 25.6	115 ± 21.4	127 ± 0.51	0.18 ± 0.006	-33 ± 1.0
OCB3	0.5:6.0	200 ± 51.5	228 ± 86.5	255 ± 2.17	0.33 ± 0.005	-34 ± 1.5

[a]Average particle sizes were obtained by ImageJ analysis (from more than 50 particles in each image and three images from 3 independent experiments were used for each material).

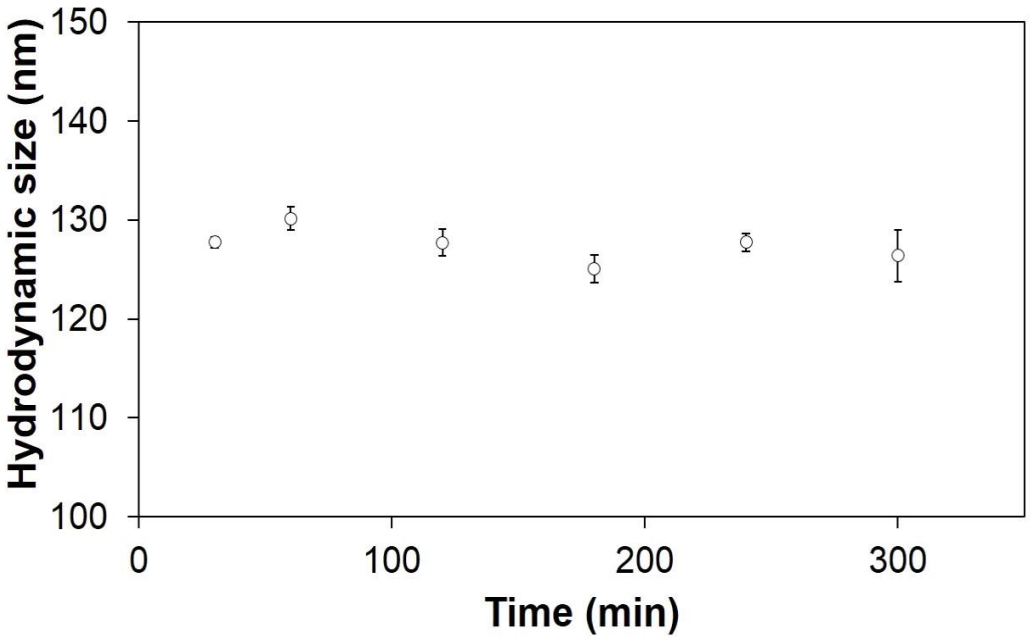

Figure 4.3 Average hydrodynamic size (shown as mean ± SD) of OCBs at various sitting times

4.2 Chemical functional groups characterization

Here, the chemical functional group of OCB2 (called as OCB) was analyzed by following techniques.

4.2.1 UV-Vis spectroscopy

The UV-visible absorption spectrum of the obtained OCBs shows maximum absorption at 244 nm with broad extension up to 600 nm (Figure 4.4), indicating the **π**-**π** conjugation of carbon networks in the OCBs.

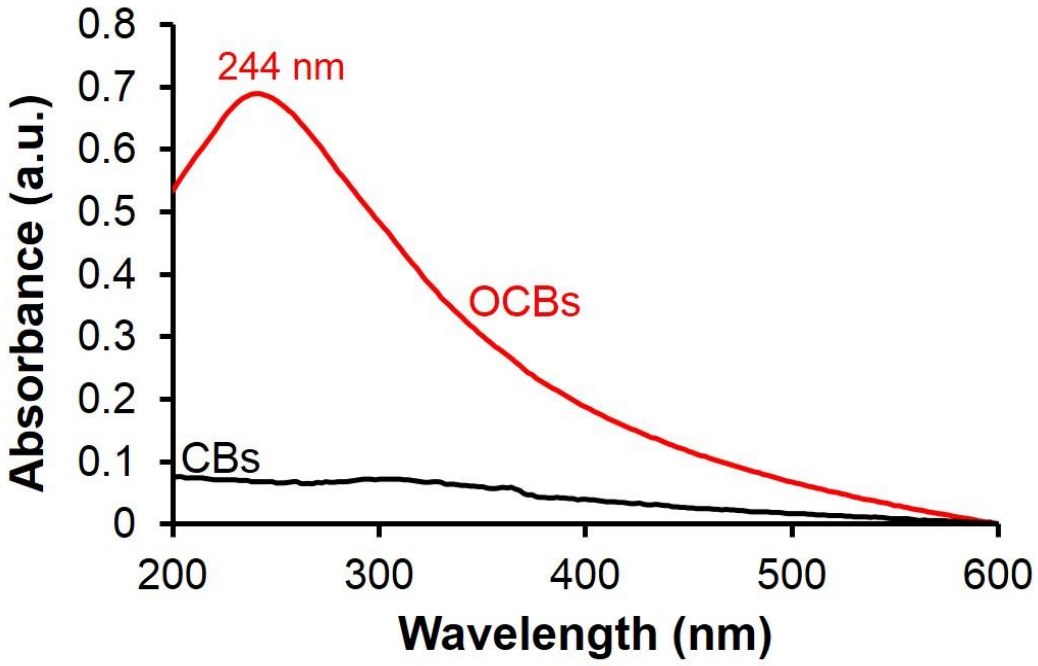

Figure 4.4 UV absorption spectra of CBs (black line) and OCBs (red line).

4.2.2. Fourier transform infrared spectroscopy (FTIR)

The FTIR spectrum of OCBs shows a broad OH stretching at 3338 cm^{-1}, C=O stretching and C=C stretching at 1600-1800 cm^{-1}, C-O stretching/ C-H bending/O-H bending at 1100 -1410 cm^{-1} (Figure 4.5).

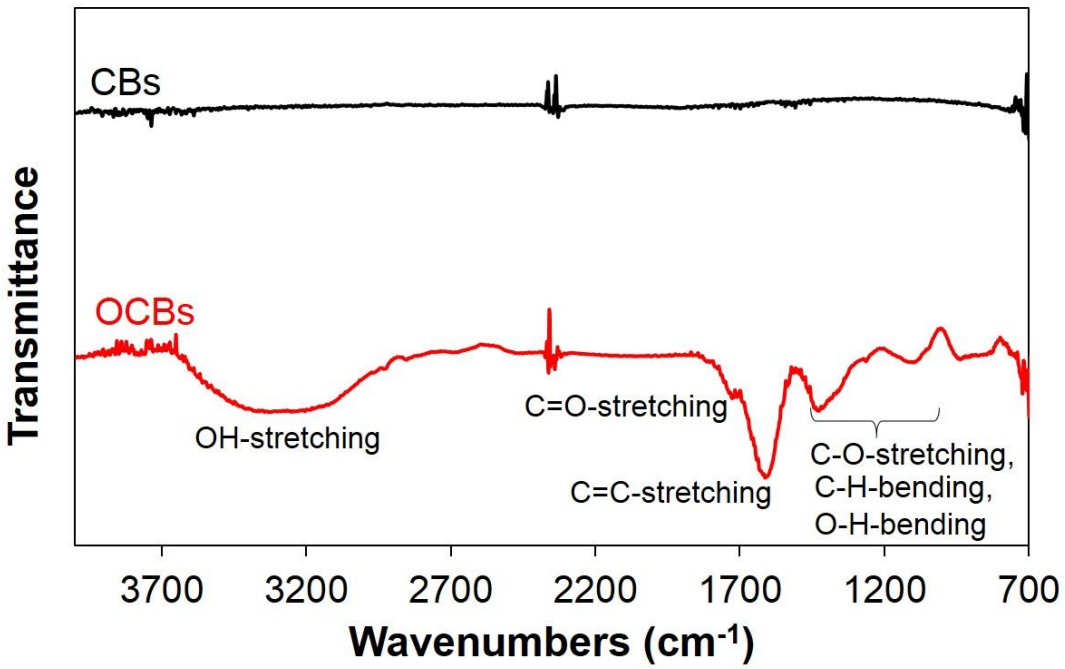

Figure 4.5 FTIR spectrum of CBs (black line) and OCBs (red line).

4.2.3. Raman spectroscopy

The structural characterization of CBs and OCBs was also carried out by Raman spectroscopy. The vibration spectra of CBs and OCBs are shown in Figure 4.6. Raman spectrum of the CB raw material shows a typical G band at ~1590 cm^{-1} (also called graphite peak), D band at ~1360 cm^{-1} (also known as sp^2 carbon disorder-induced peak), with almost undetectable 2D or G′ band at 2500-3400 cm^{-1} (disordered sp^2 planes), as expected. Here a slightly blue shift of the D-band in the OCBs spectrum, as compared to that of the CBs, can be observed (Figure 4.6). In addition, the D band to G band peak area ratio increases from 1.25 for the original CBs to 1.56 for the OCBs, indicating the structural deformation of the planar carbon (sp^2 carbon) upon the

oxidation of CBs into OCBs. Multiple broad 2D bands are also obvious in the Raman spectrum of OCBs, but are undetectable in the CB spectrum. This agrees well with the disordered carbon network planes in the OCB structure which are responsible for the multiple interlayer interactions at various depths among many disordered carbon networks.

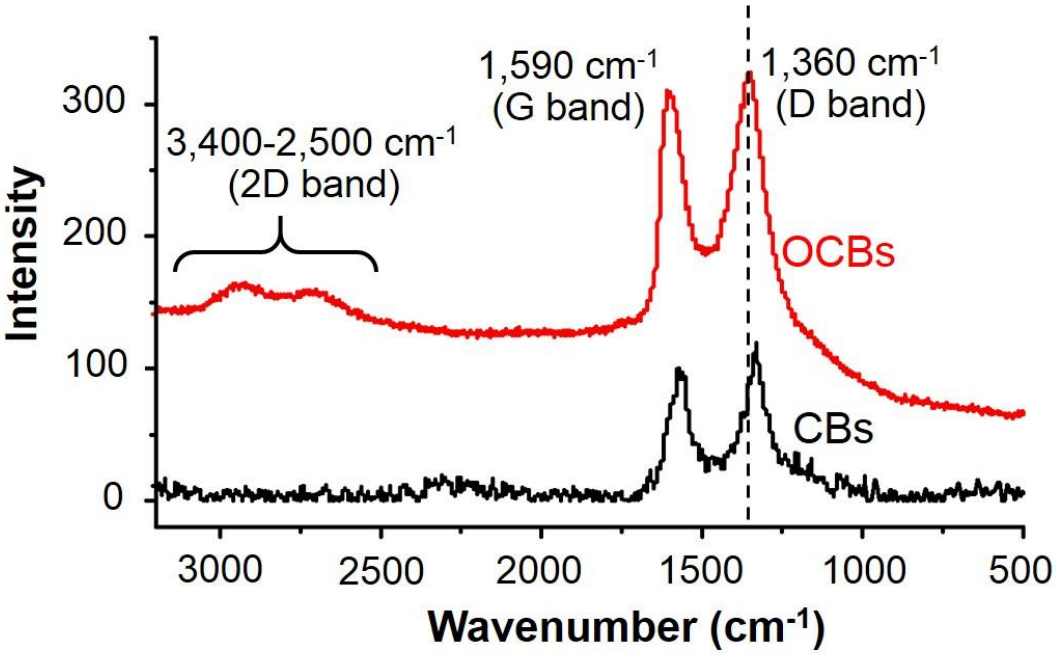

Figure 4.6 Raman spectrum of CBs (black line) and OCBs (red line).

4.2.4. X-ray photoelectron spectroscopy (XPS)

X-ray photoelectron spectroscopy (XPS) is a surface-sensitive quantitative spectroscopic technique that measures the elemental composition. A typical XPS spectrum is plot of the number of electrons detected versus the binding energy (BE) of the electrons detected. Each functional group/element produces a characteristic set of XPS peaks at characteristic binding energy values. XPS analysis can determine

the composition at the surface of the materials with binding energy values. To investigate surface functional group of OCBs, XPS analysis was used. The survey scan XPS spectra of CBs and OCBs indicate an increase in oxygen content upon the oxidation of the CBs into the OCBs (see O1s peak at 532 eV in Figure 4.7 a1 and b1); C1s and O1s spectra of the starting CBs show minute amount of C-O and C=O (Figure 4.7 a1, a2 and a3), C1s spectrum of OCBs shows high intensity peaks at the binding energy (BE) of 283.9, 285.3, 286.2, 287.5, and 289.7 eV which correlate well to the C–C, C=C, C–O (from C–O–C and C–OH), C=O, and COOH functional groups, respectively (Figure 4.7 b2); the O1s spectrum of the OCBs also shows high intensity peaks at the binding energy of 532.8, 531.6, and 530.9 eV which correspond well to the C–O (from C–O–C and C–OH), C=O and COOH functional groups, respectively (Figure 4.7 b3).

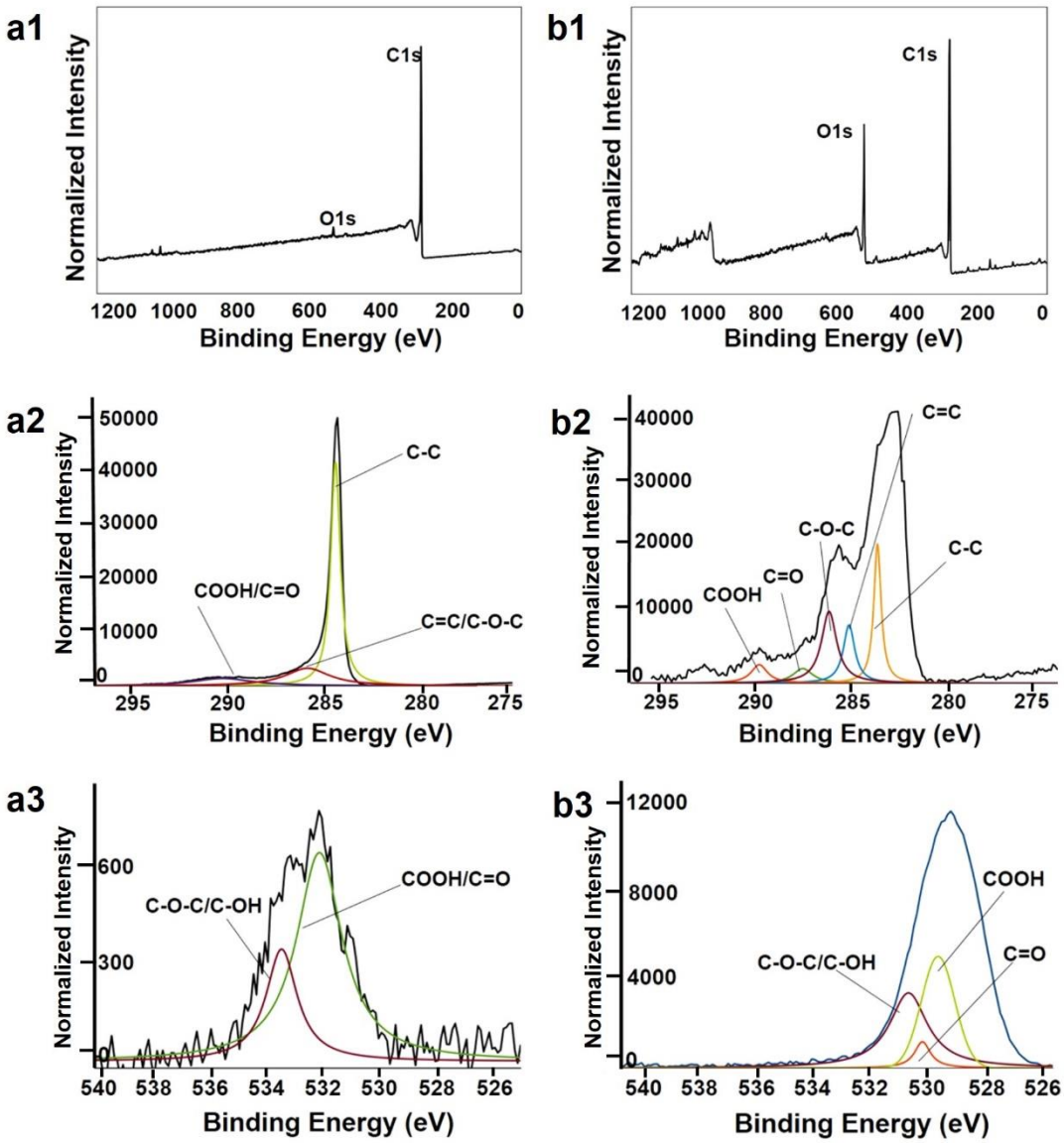

Figure 4.7 XPS spectra of CB and OCBs. Survey Scan spectra (a1 and b1), deconvoluted C1s fitting spectra (a2 and b2) and deconvoluted O1s fitting spectra (a3 and b3) of CBs (a1, a2, and a3) and OCBs (b1, b2 and b3).

4.2.5 Elemental analysis (EA)

Quantitative analysis of the elemental composition of the CBs and OCBs were identified by combustion elemental analysis. The result shows that only carbon constituent in the starting CB, whereas C, H and O at the molar ratio of 1.0: 0.27: 0.64 can be detected in the OCBs.

Based on the characterization of morphology and surface functional groups of OCBs, a reaction mechanism, whereby the carbon black agglomerate was broken down in to fine aggregate or single sphere, is being proposed and shown in Figure 4.8. Actually, There are some similarities of structure between carbon black and graphite, both consists of many graphene sheets stacked together [37]. After oxidation reaction, the outer graphene sheets (surface of CBs) were oxidized to form epoxide, carboxyl and hydroxyl functionalities on their surfaces and causing some disordered planar carbon planes. The hydrophilicity on their surfaces cause them to disperse well in water and also cause the deaggregation in this media.

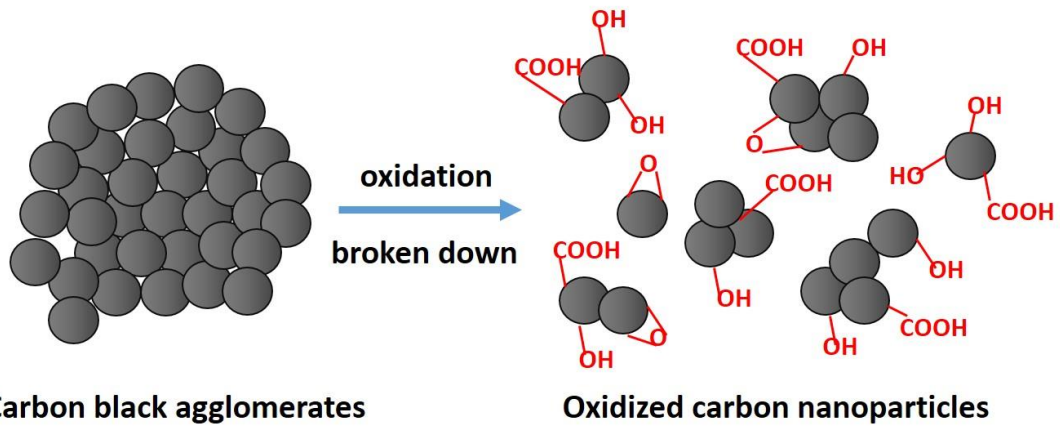

Figure 4.8 A simplified scheme of the proposed mechanism of the oxidation of carbon black.

4.3 Preparation of fluorescence dye labelling OCBs

In order to follow the intracellular localization of OCBs inside target cells, OCBs needed to be labelled with fluorescent dye. Fluorescence dye moieties with carboxyl group (5-carboxyfluorescein or fluorescein, coumarin-3-carboxylic acid or coumarin, and 5-carboxytetramethylrhodamine or TAMRA) were coupled to hydroxyl group on the oxidized carbon black surface. The carboxyl group of fluorescence dye was first reacted with EDCI to form an unstable O-acylisourea intermediate, and NHS was then acted as a proton exchanger. The intermediate continue to react with hydroxyl group of OCBs to form ester bond. Degree of the coupling of the dyes on OCBs was adjusted by trial and error (during the coupling reaction) to be in the same rage (20-30%). Here, we obtained fluorescein-labelled OCBs (flu-OCBs), coumarin-labelled OCBs (cou-OCBs) and TAMRA-labelled OCBs (TAMRA-OCBs) for use in further experiments.

4.4. Penetration of OCBs into liposome

The penetration of OCBs across lipid bilayer membrane was investigated by incubating flu-OCBs with artificial cells (cell-sized liposomes) constructed from phospholipids commonly found in membranes of living cells [39, 40]. The experiment was started by flu-OCBs with cell-sized liposomes under the confocal laser fluorescence microscopic (CLFM) observation. At the beginning, the fluorescence signals inside of liposome was not observed (Figure 4.9a, 0 min). However, after 30 min

incubation, the fluorescence signal at the inside of the liposome was very obvious, and its intensity kept increasing along the incubation time (Figure 4.9 a and b). The result indicates that the OCBs can penetrate into the inside of the liposomes without the deformation of lipid bilayer wall of the liposomes.

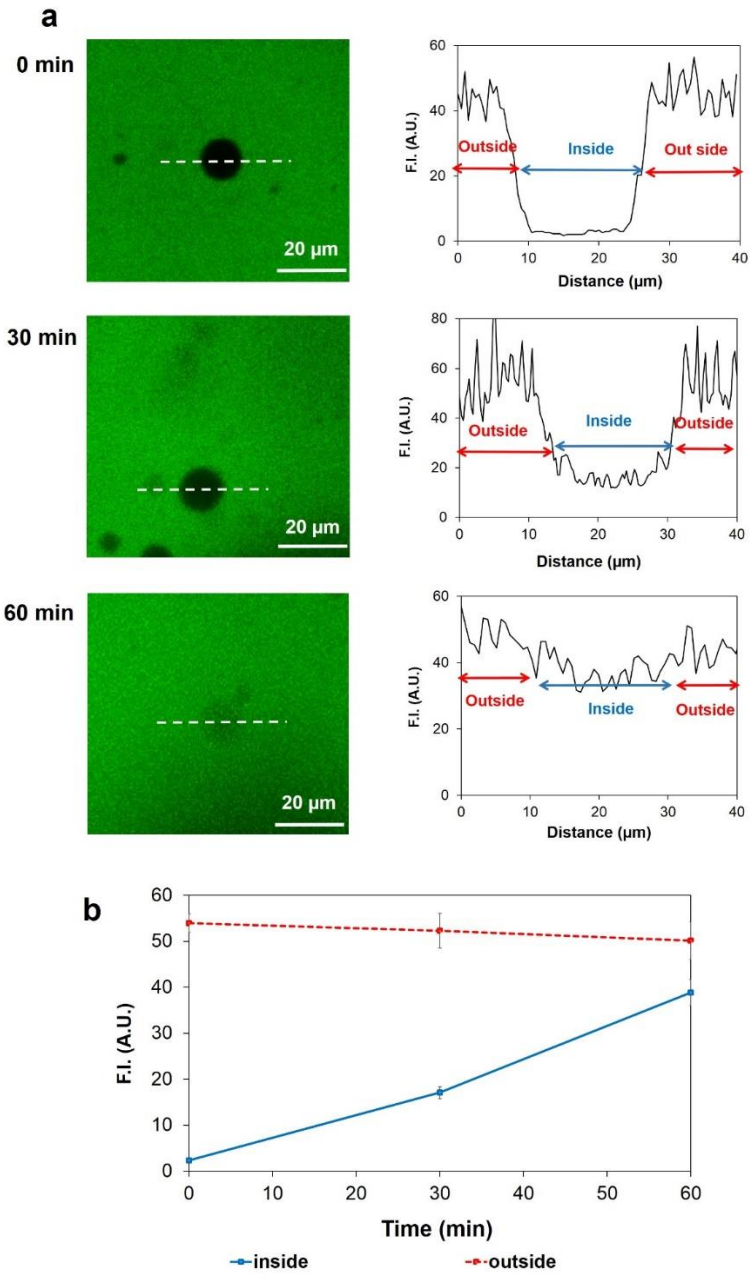

Figure 4.9 Liposome leakage. Penetration of flu-OCB into liposomes (a) Fluorescence images of liposomes after being incubated with flu-OCBs (in green) for 0, 30 and 60 min (left) accompanied with plots of fluorescence intensity (F.I.) along the dotted line of the corresponding liposomes (right), (b) A plot of F.I. from flu-OCBs at the inside and outside of the liposomes, as a function of incubation time (shown as mean ± SD).

4.5. Anthocyanin leakage by OCBs

Next we investigated the ability of OCBs to induce leakages on liposome wall. Here we investigated whether the OCBs could induce leakage of dye out of the liposomes. Liposomes filled with anthocyanin were prepared and then OCBs were introduced into the system at the outside of the anthocyanin-filled liposomes. We monitored the fluorescence signal of anthocyanin at the inside and outside of liposomes. At first, the fluorescence of anthocyanin outside the liposomes was undetectable (Figure 4.10a, 0 min), corresponding well to the fact that all the dye molecules were initially inside the liposomes. Further incubation with the OCBs, the emission from anthocyanin at the inside of the liposomes decreased and that at the outside of the liposomes increased (Figure 4.10a and b). At 30 min, fluorescence at the outside was very obvious. In the control experiment (no OCB), no fluorescence signal was observed at the outside of the liposomes even after 1 h post OCB addition. This result indicates that OCBs can induce leaks on the liposome membrane. At the concentration of the OCB used in this experiment (100 μg/mL), the numbers of liposomes left in the systems after 60 min incubation were the same for both the

system with added OCBs and the system without OCB addition, indicating that the OCB, although could induce the liposome leak, did not significantly induce the liposome break. This result confirms the ability of the OCB to induce leakage on phospholipid bilayer membrane without causing a significant liposome break.

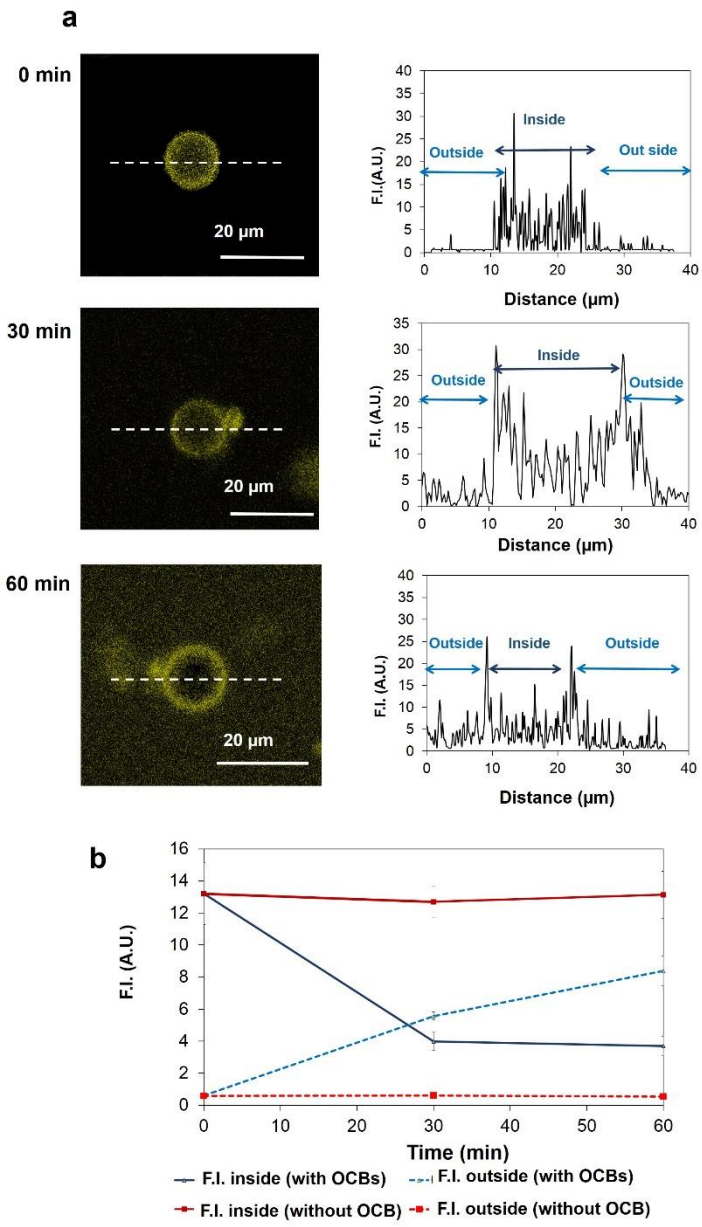

Figure 4.10 Anthocyanin leak from liposomes (a) Fluorescence images of anthocyanin (yellow) filled liposomes after being incubated with OCBs for 0, 30 and 60 min (left)

accompanied with plots of F.I. along the dotted line of the corresponding liposomes (right), (b) A plot of anthocyanin F.I. at the inside and outside of the anthocyanin filled liposomes after water addition (without OCB) or OCBs addition (with OCBs), as a function of incubation time (shown as mean ±SD).

4.6. Adsorption of phospholipids on OCBs

From previous experiment, we found that the OCBs can induce leakage on phospholipid bilayer membrane. We speculated that the leak is caused by an adsorption of lipid molecules to OCB's surfaces. Therefore, here we investigated adsorptions of various molecules onto the OCBs. The experiment was carried out by observing changes in sizes of the OCBs after being incubated with different tested materials. DLS measurement was used for the particle size determination. The result indeed showed that hydrodynamic size and zeta potential of OCBs significantly increased upon incubation with different compounds ($p < 0.05$, Figure 4.11a and b). The two tested phospholipids, DOPC and Egg PC, and a hen egg lysozyme protein induced the most size changes to the OCBs. It should be noted here that the two lipids are the main constituents of most living cell membrane [39, 40]. The increase in hydrodynamic size of OCBs was likely to be caused by adsorption of the tested materials onto the particle's surface. The BSA (66 kDa) and cholesterol also induced significant size changes, although at a lesser extent than the two lipids. Nevertheless, PDI of the particles was not affected by any of the material adsorptions. It should be

noted here that, after incubating the OCBs particles with the tested materials, all the particles still dispersed well in water. The OCBs particles seems to have high surface energy and can adsorb various materials to their surface, with the preference of adsorbing phospholipids. This preference may relate to the particle's ability to induce leak on the phospholipid bilayer membrane. Further investigation the leakage mechanism is needed.

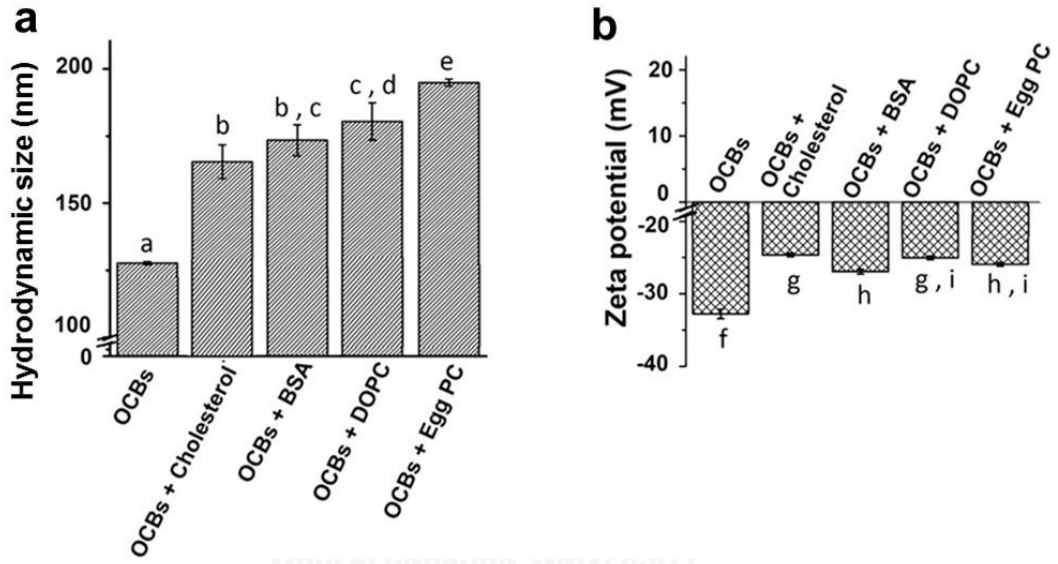

Figure 4.11 Hydrodynamic sizes (a) and zeta potentials (b) of OCBs before and after incubation with various molecules. Data are shown as the mean ± SD and different alphabets on the data bars indicate significant statistical difference (same alphabet means "not significant different"), as determined by one way ANOVA Tukey at $P < 0.05$.

4.7. Cellular trafficking of protein and OCBs

With the ability of OCBs to induce phospholipid bilayer membrane leak in the cell-sized liposomes, we further investigated whether the particles could do the same on membranes of living cells. Also we were interesting to see if the OCBs could leak

big protein molecules into cells. Therefore, ability of the OCBs particles to leak into the CaSki cells was explored, and ability of the particles to bring hen egg white lysozyme protein (MW of 300 kDa) into the CaSki cells was also investigated.

Flu-lysozyme and cou-OCBs were used in this experiment. To investigate whether the penetration of the tested materials into cells occurred via direct phospholipid bilayer membrane penetration or via endocytosis, we also monitored the location of the endosomes and lysosomes during the particle uptake experiments using the dyes specific to these two organelles.

The fluorescence signals observed under CLFM at 45 min after incubating the flu-lysozyme and cou-OCBs with CaSki cells indicated that the protein and the carbon particles were taken up into the cells (purple color for cou-OCBs (column 1) and green color for flu-lysozyme (column 2) as shown in Figure 4.12. Locations of endosomes and lysosomes are unrelated to the locations of the OCBs and the lysozymes, thus implying that these materials were not taken into the two subcellular organelles. The result implies direct penetration of the two materials across phospholipid bilayer membrane of the cells, into the cells' interior. It should be noted here that when the cells were incubated with only flu-lysozyme (no cou-OCB), no fluorescence signal of the protein could be observed inside the cells even after 45 min of incubation (Figure 4.13). The result agrees well with the ability of the OCBs to induce leakage of phospholipid bilayer membrane of the cell-size liposome. Therefore, here we clearly

demonstrate that the OCBs can directly penetrate CaSki cells' membrane and also efficiently and quickly allow the 300 kDa protein to directly enter the cells.

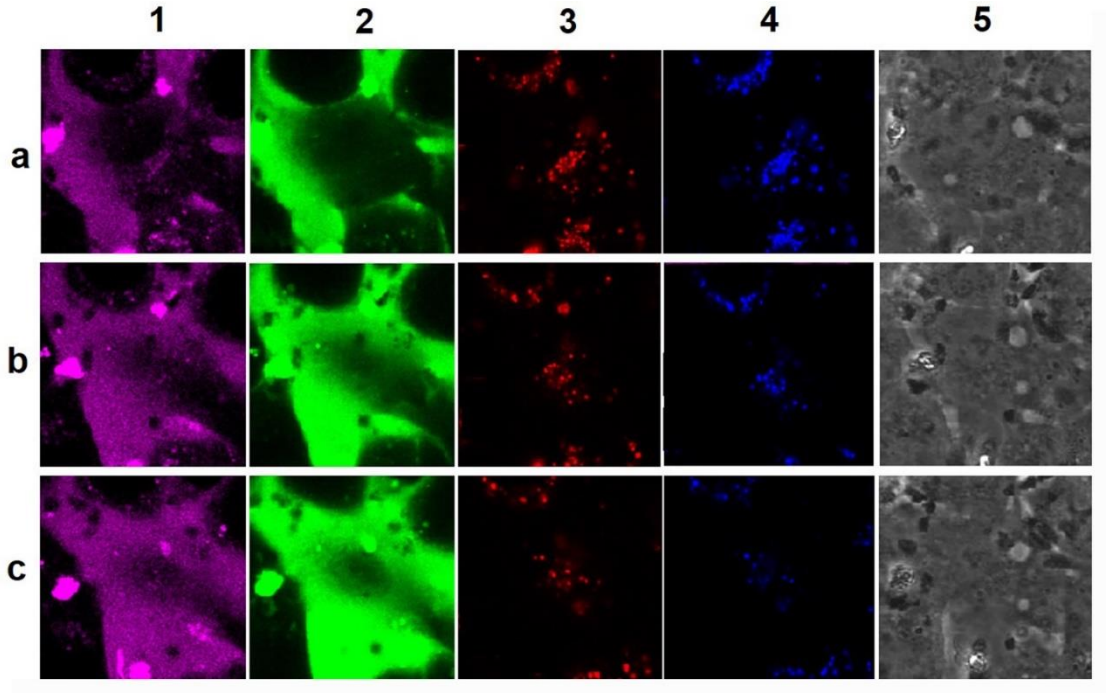

Figure 4.12 Trafficking of flu-lysozyme protein and cou-OCBs in CaSki cells. CLFM images of CaSki cells after being incubated with flu-lysozyme protein plus cou-OCBs for 15 (row a), 30 (row b), and 45 (row c) min: Signals from cou-OCBs in magenta (column 1), flu-lysozyme protein in green (column 2), early endosome in red (column 3) and lysosome in blue (column 4). Corresponding cell images under phase contrast mode at 45 min incubation time are shown in column 5.

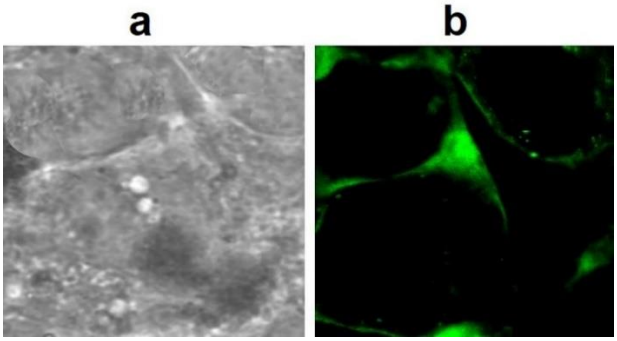

Figure 4.13 CLFM images of CaSki cells after being incubated with only flu-lysozyme (no OCB) for 45 min: (a) Cells morphology in phase contrast mode and (b) Similar image in fluorescence mode with fluorescence signals from flu-lysozyme protein in green.

4.8. Cellular uptake of OCBs and protein

From the cellular trafficking of protein and OCBs observation, the results clearly indicate that the OCBs can directly penetrate cell membranes and allow big protein molecules to straightly enter cells. Therefore, it will be interesting to observe the location of these materials after a long incubation time and also relate their location to the nucleus. Here, we first investigated for the location of the OCBs inside the cells using two different cells, RAW 264.7 and CaSki cells line.

In order to incubate OCBs with the cell for a long time, the cytotoxicity of OCBs was necessary to investigate. Here, the cytotoxicity of OCBs was investigated by using MTT method. When RAW 264.7 and CaSki cells were cultured *in vitro* with the OCBs at concentrations of 0.1–1.0 μg/mL for 48 h, no significant cytotoxicity was detected. The results show cell viabilities of RAW 264.7 and CaSki cells were approximately 90% and 96%, respectively. Cell viabilities of more than 80% were attained in the presence of

3.2 μg/mL OCBs for RAW 264.7 cells or 10 μg/mL OCBs for CaSki cells (Figure 4.14). This relatively low *in vitro* cytotoxicity of the OCBs indicates the material's biocompatibility, therefore, inspiring applications of the OCB as a carrier to bring protein into cells.

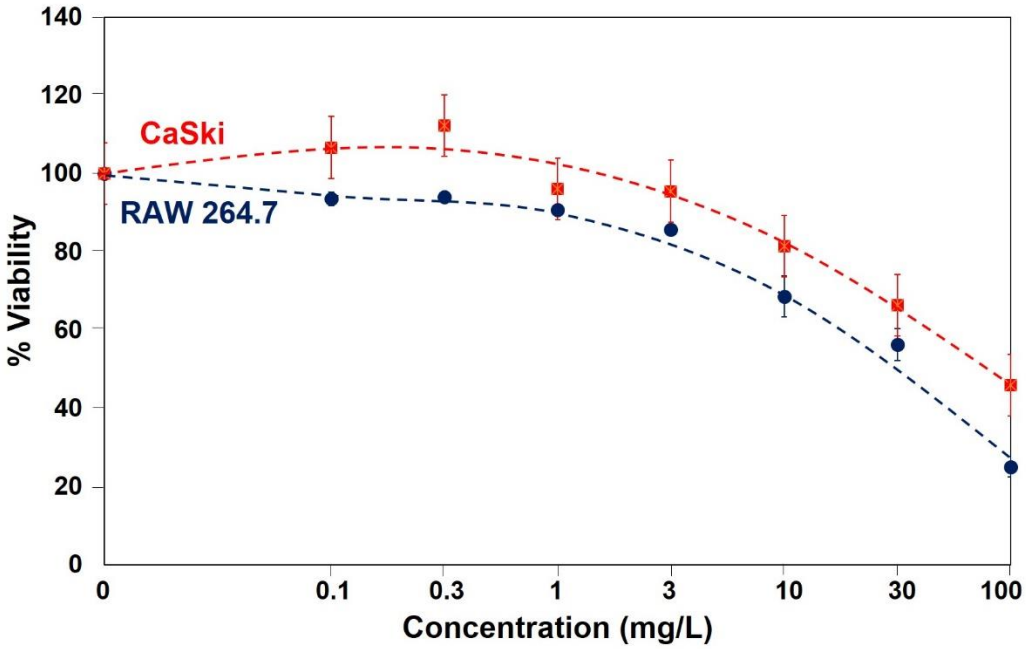

Figure 4.14 In vitro cytotoxicity of OCBs. RAW 264.7 (blue line) and CaSki cells (red line) after a 48 h exposure to various concentrations of OCBs, as evaluated by an MTT assay. Data are shown as the mean ± SD and are derived from three independent repeats.

To follow the OCBs inside the cells, we used TAMRA-OCBs in this experiment. The cells were incubated with TAMRA-OCBs for 4 h and then thoroughly washed before being subjected to the fixation process to stain cell's nuclei with DAPI. Then the fixed cells were subjected to CLFM analysis. The fluorescence signal of the TAMRA-OCBs

could clearly be detected in the cytoplasm and nucleus of the two cells (Figure 4.15a for RAW 264.7 and 4.13b for CaSki cells), indicating that the OCBs particles can penetrate not only the cell membrane, but also the nuclear membrane.

We know from the above CLFM live-cell experiments that the big lysozyme protein can be delivered into cells by the OCBs and the delivery route is not through the endocytosis, but rather the direct leakage of the protein across the cell membrane. In addition, by fixing cells with DAPI, we know that the OCBs can be accumulated at the nucleus after 4 h incubation. We further investigated for the location of the proteins which had been delivered into cells by the OCBs. We incubated the flu-lysozyme and OCBs with the CaSki cells for 4 h and subjecting the cells to washing and nuclear staining processes, then the fixed cells were observed under a CLFM. The result shows no signal of the flu-lysozyme in the cells when OCB was not used (Figure 4.13c). In contrast, in the presence of both the protein and OCBs, obvious fluorescence signal of the flu-lysozyme could be seen at the cytoplasm and nucleus of the cells (Figure 4.15d). The result here implies that the OCBs can effectively deliver lysozyme into nucleus of cells.

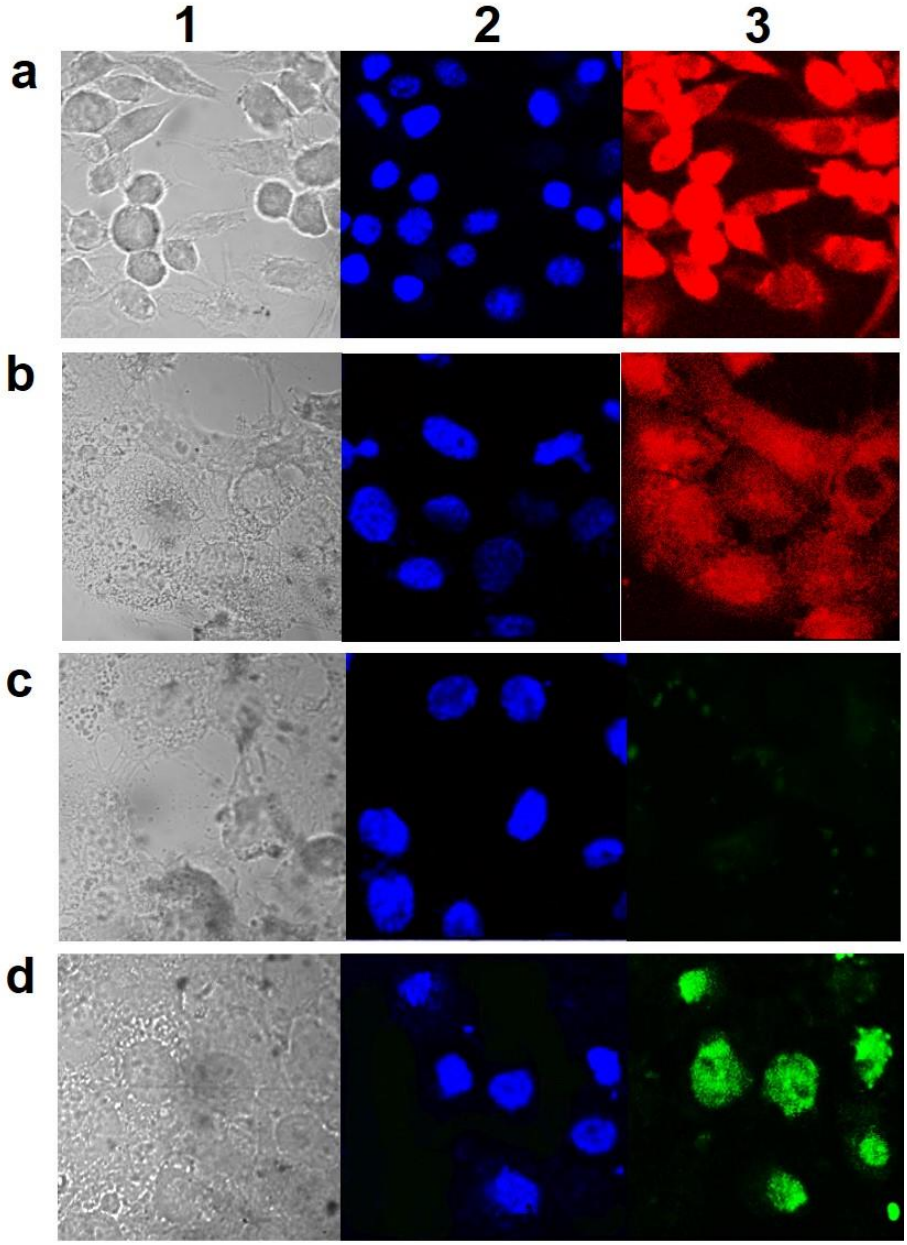

Figure 4.15 Cell membrane and nuclear membrane penetration of OCBs. CLFM images of RAW 264.7 (row a) and CaSki (row b, c and d) cells after being incubated for 240 min with TAMRA-OCBs (Row a and b), flu-lysozyme (row c), and flu-lysozyme plus OCBs (row d).

According to the result above, OCBs could directly deliver big functional proteins across cell membranes via a non-endocytic pathway. Next, we study the ability of OCBs to enhance phospholipid bilayer membrane passage of both micro sized and nano sized particles.

4.10. Preparation and characterization of micro/nanoparticles

Here we used the retinal-grafted chitosan particles of various sizes as model particles to investigate an ability of the OCBs to bring particles into cells. We selected these particles because of a few reasons. First, the particles are auto-fluorescent, thus allowing us to monitor them under confocal laser fluorescence microscope (CLFM). Secondly, it has been known that chitosan is the polymer that possesses good cellular uptake character [41], therefore an ability to enhance the particles made from chitosan should demonstrate real interesting efficiency enhancement. Thirdly, since the retinal-grafted chitosan particles (or the so-called pro-retinal particles or PRPs) can be used for therapeutic aspect inside the cells, enhancing their cellular uptake efficiency may have a direct impact for applications [34, 42]. The pro-retinal micro/nanoparticles (PRPs) were prepared by grafting retinal onto *N*-succinylchitosan. The amine groups of N-SC moiety were reacted with aldehyde groups of retinaldehyde to produce amide bond (Schiff base). Then, the yellow suspension of PRPs was obtained. The PRP product was separated using step-wise centrifugation to obtain particles of different sizes. SEM images (Figure 4.16) indicate that we have obtained the PRPs of three

different sizes were 1000 ± 82.5 nm (PRP1), 500 ± 22.7 nm (PRP2) and 390 ± 15.5 nm (PRP3) (estimated sized from their SEM images). These sizes corresponded well with the average hydrodynamic sizes (obtained from DLS) of PRP1, PRP2 and PRP3 were 1200 ± 51.5 nm , 540 ± 29.0 nm and 430 ± 11.0 nm, respectively. All the three sized PRP particles possess similar zeta potential of 50 ± 0.5 mV.

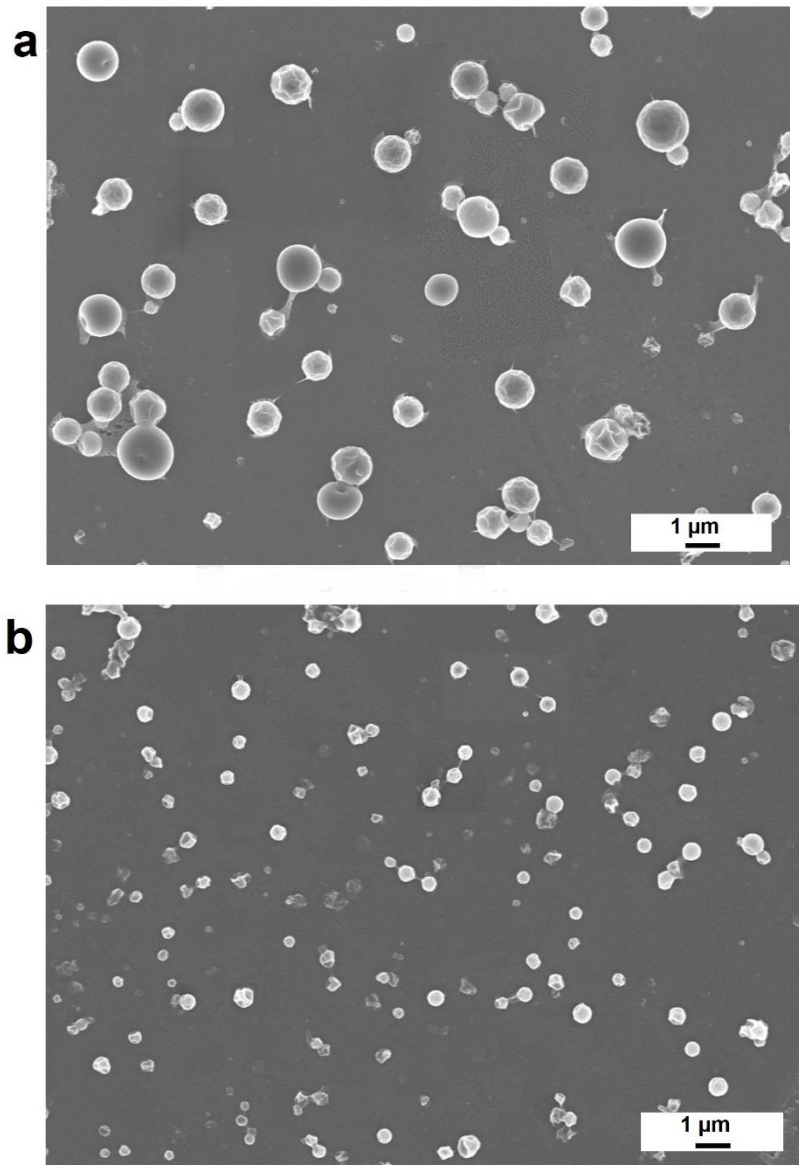

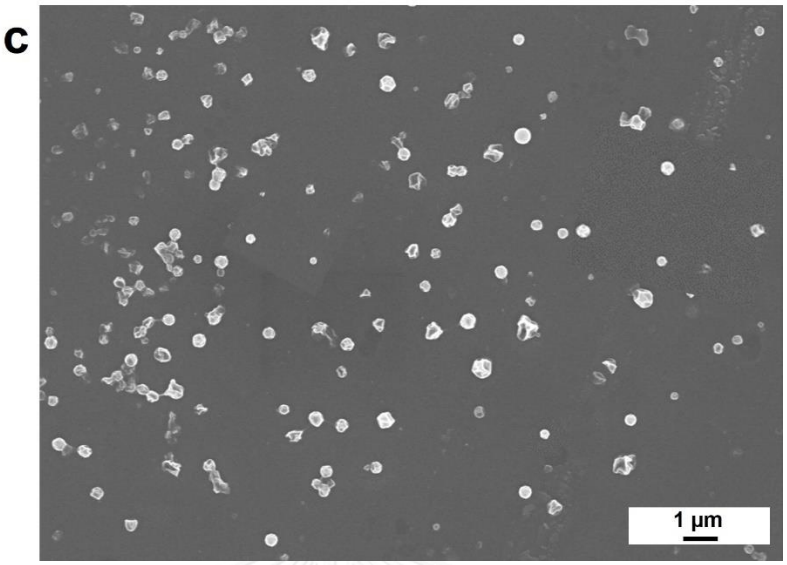

Figure 4.16 Morphology of the three sized pro-retinal particles (PRPs). SEM images of PRP1 (a), PRP2 (b) and PRP3 (c).

4.11. Penetration of PRPs into cell-sized liposomes

The different sized PRPs were tested for their ability to penetrate across lipid bilayer membrane using artificial cells (cell-sized liposomes). The use of the giant liposome makes it possible to focus only on passive transport across the membrane with no involvement from active trans-membrane protein. We prepared the artificial cells with phospholipid using the hydration technique as previously described. We then incubated the prepared cell-sized liposomes with PRPs and monitored fluorescence signals of PRPs at the inside and outside of liposomes as a function of incubation time, using a CLFM. We observed that the PRP2 and PRP3 were adsorbed on the surface of the liposomes after 30 min incubation and the two sized particles

could penetrate into the inside of the liposome after 45 min incubation (Figure 4.17). In the case of the PRP1, the fluorescence signal of the particles on the liposomes was undetectable even after 90 min incubation, thus implying minimal to no interaction between the PRP1 and the liposomes. These results indicate that the 400-500 nm sized PRPs (PRP2 and PRP3) penetrate phospholipid bilayer membrane more effectively than the 1200 nm PRPs (PRP1).

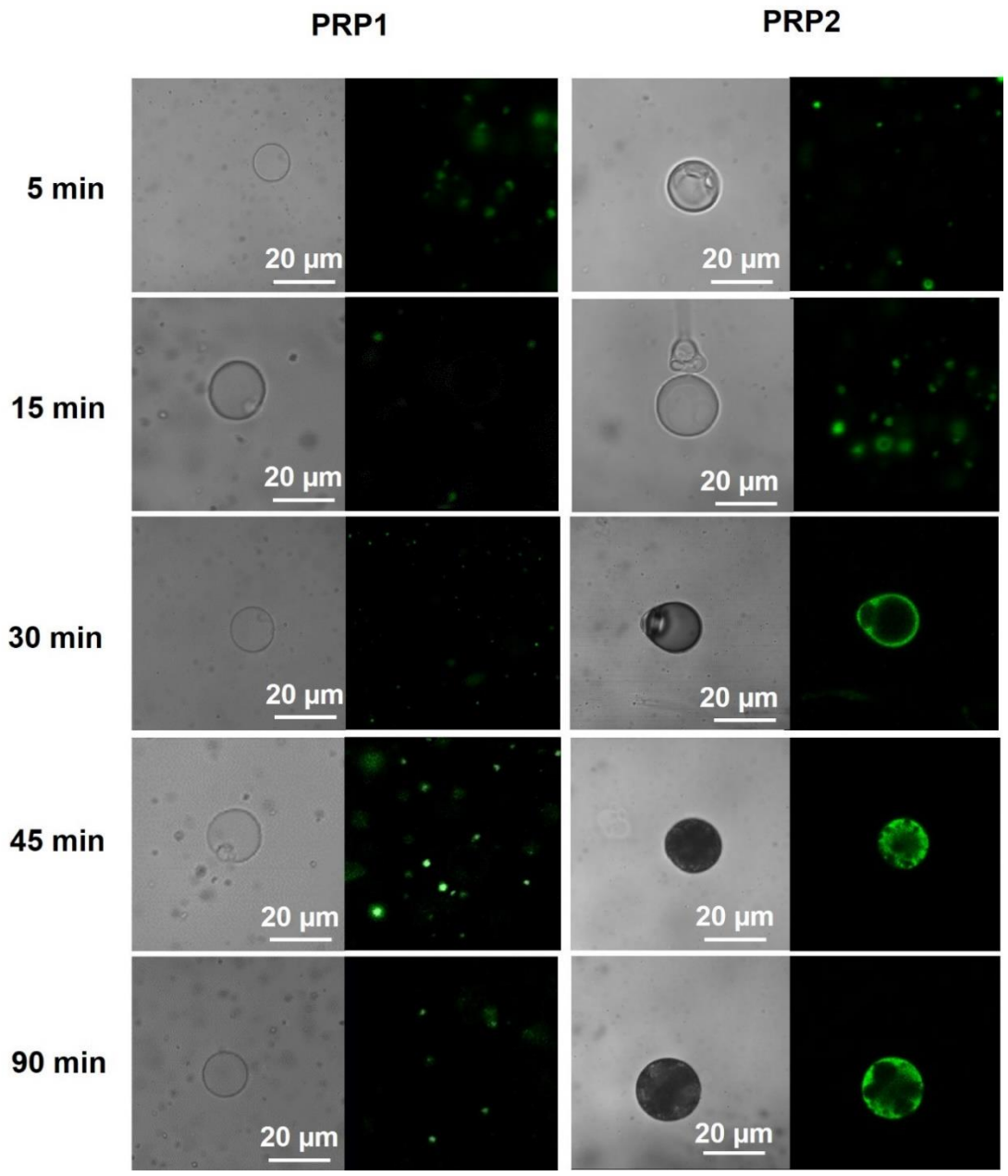
PRP1
PRP2
5 min
15 min
30 min
45 min
90 min
20 µm

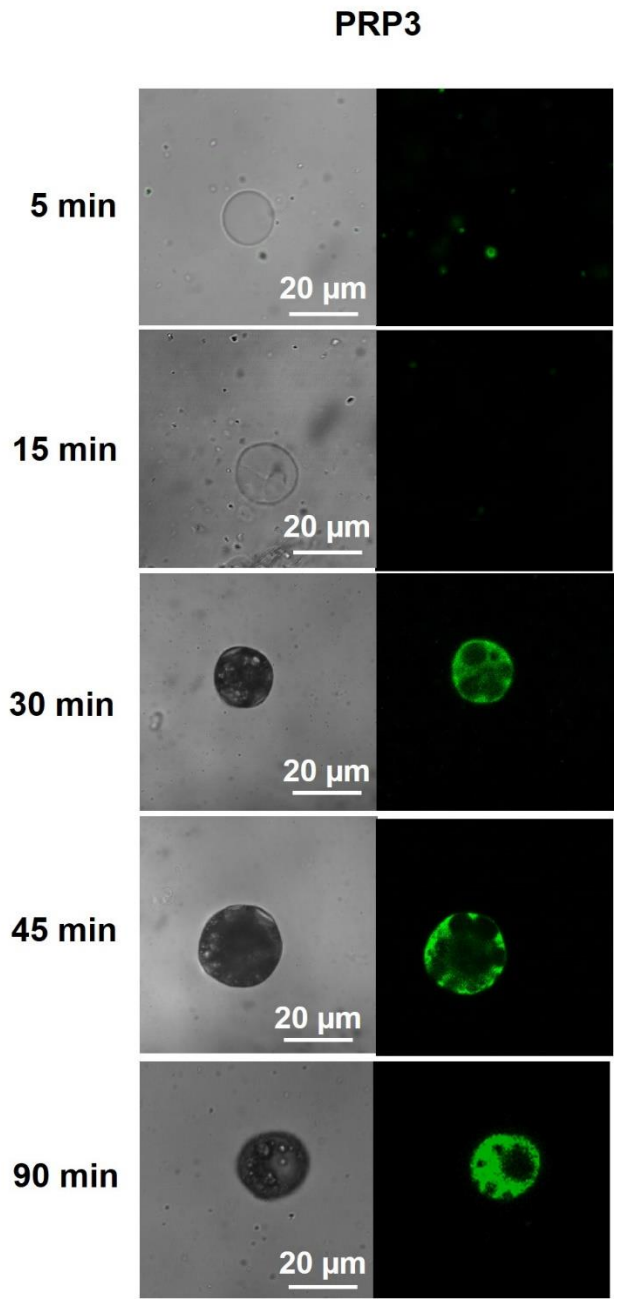

Figure 4.17 PRPs micro/nano particles penetrated into liposomes without the presence of OCBs. CLFM images representative liposomes morphology (left) and fluorescence signal of PRPs in green (right). The results are shown as the function of incubation times from 5 to 90 min.

4.12. Using OCBs to deliver PRPs into cell-sized liposomes

Here we tested whether OCBs could increase the lipid bilayer membrane penetration of the PRPs. OCBs and PRPs were mixed (mass ratio of OCBs: PRPs of 1:4) then incubated with liposomes, the fluorescence signal of the PRPs was monitored by CLFM. The results show that in the presence of OCBs, the fluorescence signals of the PRP1 could be observed at the surface of the liposomes within 5 min after incubation and at the inside of the liposomes after 30 min incubation (Figure 4.18). Comparing to the experiment with the absence of OCB (section 4.11) in which no signal was observed at the liposome after 90 min incubation (Figure 4.17), here OCBs not only enabled the PRP1 to associate quickly to the surface of the liposome but also facilitated their penetration into the liposomes' interior.

In case of the PRP2 and PRP3, fluorescence signals of the particles were observed at the surface and at the inside of the liposomes after 5 min incubation (Figure 4.18). Comparing to 45 min requirement for the PRPs to penetrate the liposomes when there was no OCB (Figure 4.17), here the enhancement in penetration rate was very obvious. Therefore, we conclude that OCBs can enhance the association rate between the giant liposomes and the PRPs of all sizes, and can increase the penetration of all three sized PRPs into the liposomes.

It should be noted here that the prepared cell-sized liposomes were mostly multilayer liposomes. Interestingly, when these liposomes were incubated with PRP2

and PRP3 (no OCB), we observed the PRP fluorescence signals at only the first layer interior of the liposomes (Figure 4.17). This indicate that the PRPs can penetrate only the first layer of the liposomes. In contrast, in the presence of OCBs, fluorescence signals of PRPs although were observed only at the first layer of the liposomes at the beginning (Figure 4.18), further incubation quickly showed the signals at all layers of the liposomes (Figure 4.18). This indicated that the OCBs could aid the PRPs penetrate to all layers of the multilayered liposomes.

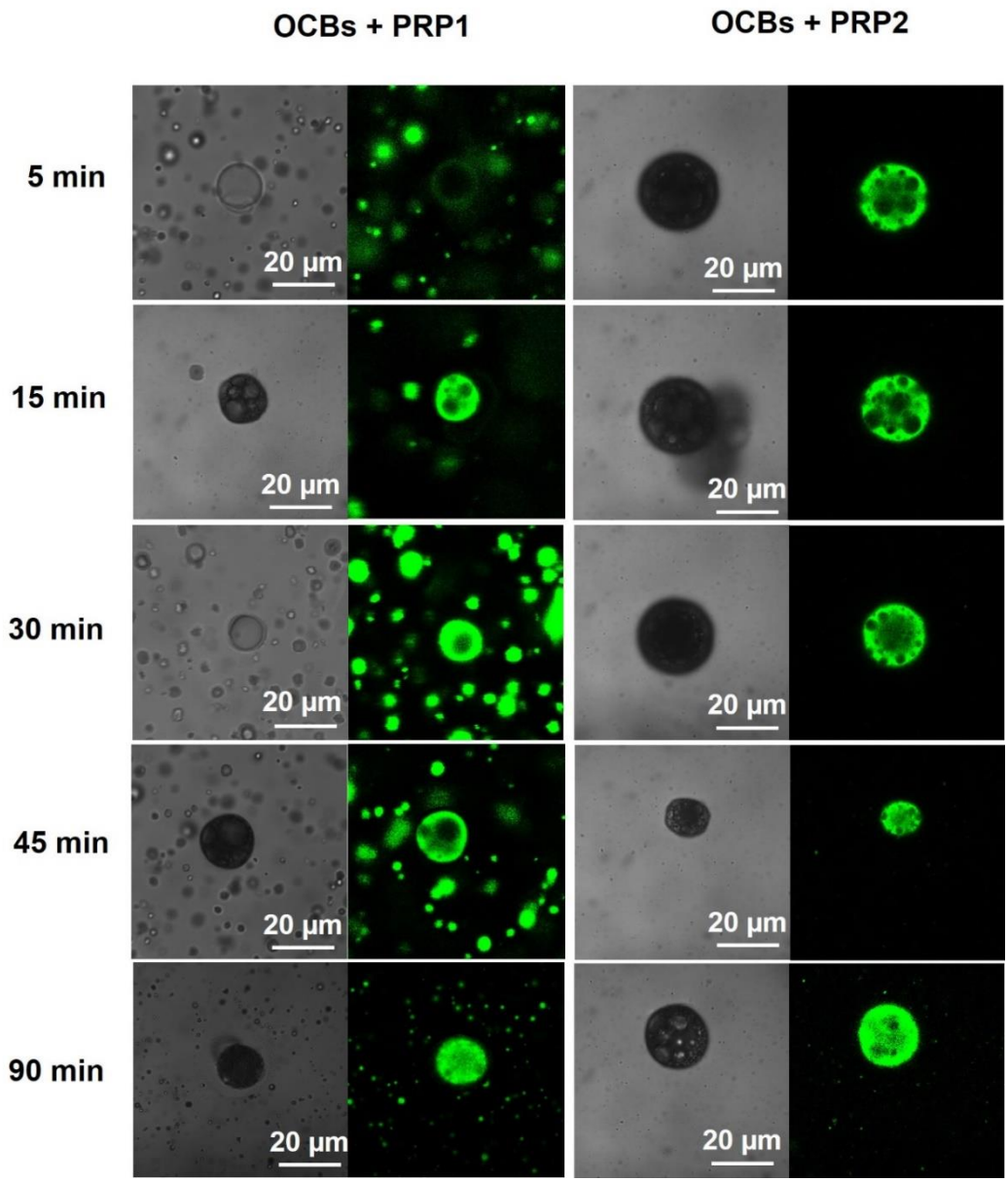
OCBs + PRP1
OCBs + PRP2
5 min
15 min
30 min
45 min
90 min
20 µm

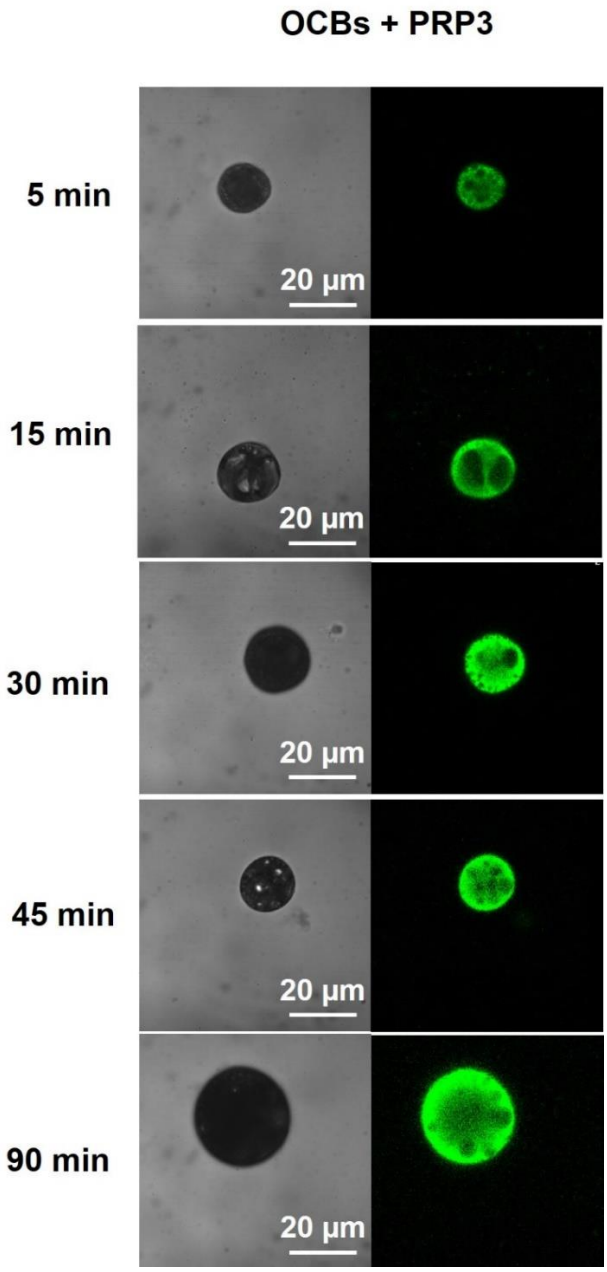

Figure 4.18 PRPs micro/nano particles penetrated into liposomes with the presence of OCBs. CLFM images representative liposomes morphology (left) and fluorescence signal of PRPs in green (right). The results are shown as the function of incubation times from 5 to 90 min.

4.13. Cellular uptake of PRPs

The abilities of the OCBs to deliver micro/nanoparticles into cells were investigated with keratinocyte cell. Cytotoxicity of OCBs were investigated quantitatively by MTT assay in keratinocyte cells at up to 30 μg/mL OCBs (Figure 4.19).

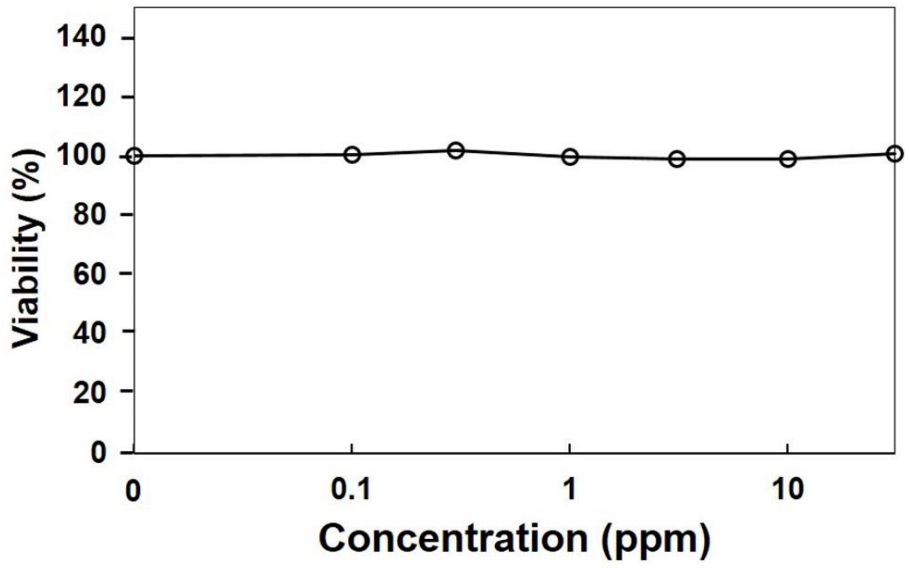

Figure 4.19 In vitro cytotoxicity of OCBs in keratinocyte cells after a 48 h exposure. Data are shown as the mean ± SD and are derived from three independent repeats.

In order to observe effect of the OCBs on the cell membrane penetration of the particles, keratinocytes were incubated with the PRPs in two different conditions, with (Figure 4.20, row 1-4) and without the OCBs (Figure 4.20, row 5-8)), for 24 h. After incubation, the cells were washed and fixed then fluorescence signals of the PRP in the cells were observed with CLFM. Fluorescence images of the cells incubated with each of the three sized PRPs (Figure 4.20 row 2-4) barely showed fluorescence signals

of PRPs in the cells. This results indicate that without OCBs, all three sized PRPs could not significantly penetrate into cells. Interestingly, the fluorescence signals from PRPs inside the keratinocyte cells significantly increased when OCBs were presence (Figure 4.20 row 6-8). Without an addition of OCB, the numbers of keratinocyte cells with detectable PRP fluorescence signal were ~ 9.5%, for all three sized PRPs. In the presence of OCBs, the numbers of keratinocyte cells with PRP fluorescence in their interior were ~ 93.6% for the PRP1, and ~ 100% for the PRP2 and PRP3. These results clearly imply that OCBs can deliver both the 1200 nm and the 500/400 nm sized PRPs into the cells.

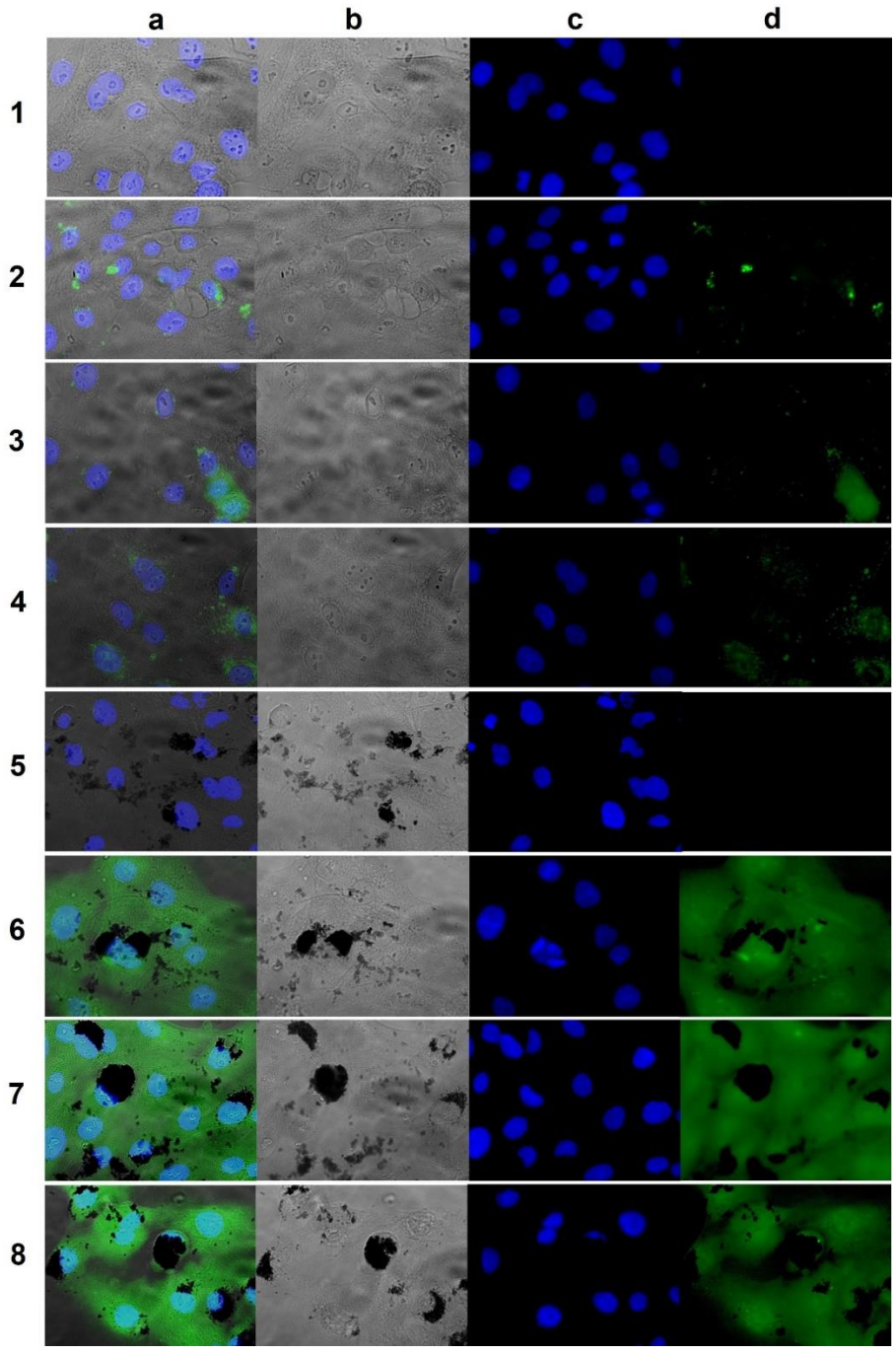

Figure 4.20 Cellular delivery of PRPs by OCBs. Fluorescence microscopic images of keratinocyte cells after being incubated with media (row 1), PRP1 (row 2), PRP2 (row 3), PRP3 (row 4), OCBs (row 5), PRP1 plus OCBs (row 6), PRP2 plus OCBs (row 7) and PRP3 plus OCBs (row 8). Un-separated images are in column a, cells morphology images

are in column b, fluorescence images showing DAPI-stained nucleus are in column c, and fluorescence images of the PRPs are in column d.

4.14. Cellular uptake and OCBs delivery of micro/nano particles into human liver cancer cells (Hep G2)

Since the keratinocytes do not take up PRP without the aid of OCBs, we investigated an effect of the OCBs over the intracellular trafficking of PRPs using HepG2. The HepG2 cells were incubated with the PRP2 (in the presence and absence of OCBs) for 30 and 60 min, then the PRP locations in the cells were identified through the particles' auto fluorescence signals, whereas the locations of nucleus, endosomes and lysosomes compartments were determined through the fluorescence signals of the dyes specific to these three organelles (DAPI for nuclei, early endosome-RFP for endosome and lysotracker for lysosome). CLFM images of HepG2 cells incubated with PRP2 (no OCB) for 30 min (Figure 4.21 row 2) showed no signal of PRP fluorescence in the cells. However, after 60 min incubation (Figure 4.21 row 3), the signals of PRP fluorescence were detected at the same locations of fluorescence signals from endosome specific dyes, implying that the PRPs were in the endosomes inside the cells. This implied that the PRPs were endocytosed into the cells. When the cells were incubated with PRPs plus OCBs for 30 min, the fluorescence signal of PRPs were detected in cytoplasm and nucleus of the cells (Figure 4.21 row4). In addition, here PRP fluorescence locations were related to neither the locations of endosomes nor

the locations of lysosomes. The result implies that the cellular uptake of PRPs in the presence of OCBs is faster and more effective than that in the absent of OCBs. More importantly, with OCBs, the particle uptake by the cells seems to be unrelated to cellular endocytosis process.

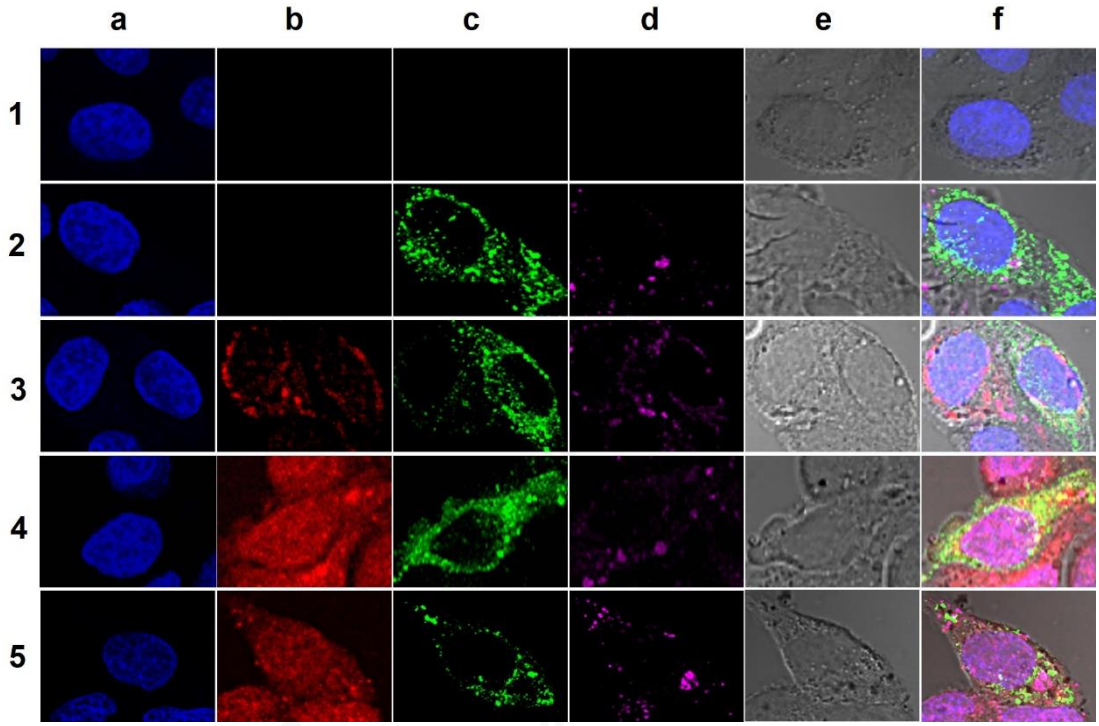

Figure 4.21 Cellular penetration of the PRP2. CLFM images of HepG2 cells after being incubated with media for 60 min (control, row 1), with PRP2 for 30 (row 2) and 60 (row 3) min, with PRP2 plus OCBs for 30 (row 4) and 60 (row 5) min: Images are shown as fluorescence images of signals indicating nucleus (blue, column A), PRP2 particles (red, column B), early endosome (green, column C), lysosome (magenta, column D), and cell morphological images (column E), and original merged images (column F).

4.15. Irritation test of OCBs and PRPs

From previous experiment, the result indicates that both OCBs (at the highest tested concentration of 30 ppm) and PRPs (at the highest tested concentration of 2 ppm) are non-toxic to keratinocytes even under the condition that the OCBs help increasing the cellular uptake of the PRPs into the cells. This non-toxicity of the combined materials in the keratinocytes, but increased cellular uptake of the PRPs, indicates possible application of the materials as cellular penetration enhancer. As a result, we next tested for the toxicity of PRPs and OCBs on the three-dimensional (3D)-human skin models (EpiSkin^{TM}, EpiSkin Research Institute, Lyon, France) [35]. The results revealed the cell viabilities of higher than 50 % upon the treatments with OCBs (at the skin coverage of 0.96 $\mu g/cm^2$), PRPs (at the skin coverage of 0.064 $\mu g/cm^2$) or the OCBs/PRPs mixture (at the skin coverage of 0.96 $\mu g/cm^2$ for OCBs and 0.064 $\mu g/cm^2$ for PRPs), whereas the cell viability dropped to 8.8 ± 0.5% upon the treatment with 5% SDS (a positive control, used at the skin coverage of 1.6 mg/cm^2). The result here indicates possible application of the OCBs as a non-toxic cellular penetration enhancer toxic cellular penetration enhancer for local drug applications.

CHAPTER V
CONCLUSION

We have successfully prepared water dispersible oxidized carbon black nanoparticles (OCBs) by oxidizing of commercially available carbon black. The obtained particle was spherical with an average hydrodynamic diameter and zeta potential of 127.7 ± 0.51 nm and -33.1 ± 1.05 mV, respectively. The particles surfaces consist of carboxylic, carbonyl, hydroxyl and ether functionality. The OCBs were relatively non-toxic to RAW 264.7, CaSki and keratinocyte cells when used at proper concentrations. The OCBs can induce the leakage on phospholipid bilayer membrane of both cell-sized liposomes and real cells. OCBs can deliver hen egg white lysozyme of MW 300 kDa, into nucleus of cells. Furthermore, we have found that OCBs can speed up both of micro sized and nano sized particles to association with phospholipid bilayer membranes and can increase the penetration of micro- and nano-particles across the membrane of the liposomes. Without OCB, keratinocytes neither take up any of the both micro sized nor nano sized particles. However, in the presence of OCBs, keratinocytes effectively take up both micro- and nano-particles into cytoplasm. For HepG2, without OCBs, micro- and nano-particles get into the cells via endocytic process, however, in the presence of OCBs, these particles get into the cell via non-endocytic process, and can proceed into the cells' nucleus. It is likely that the ability of OCBs to induce the membrane leakage is related to their ability to absorb

phospholipid molecules onto their structure. The OCBs also are non-irritating when tested on the 3-D skin model. We anticipate this report of the OCBs to be a starting point for application of OCBs as cellular penetration enhancer for various particulate materials and large biological molecules.

REFERENCES

[1] James, R., Manoukian, O.S., and Kumbar, S.G. Poly(lactic acid) for delivery of bioactive macromolecules. Advanced Drug Delivery Reviews 107 (2016): 277-288.

[2] Nakase, I., Kobayashi, S., and Futaki, S. Endosome-disruptive peptides for improving cytosolic delivery of bioactive macromolecules. Peptide Science 94(6) (2010): 763-770.

[3] Wagner, E. Application of membrane-active peptides for nonviral gene delivery. Advanced Drug Delivery Reviews 38(3) (1999): 279-289.

[4] Goda, T., Goto, Y., and Ishihara, K. Cell-penetrating macromolecules: Direct penetration of amphipathic phospholipid polymers across plasma membrane of living cells. Biomaterials 31(8) (2010): 2380-2387.

[5] Conner, S.D. and Schmid, S.L. Regulated portals of entry into the cell. Nature 422(6927) (2003): 37-44.

[6] Eke, G., Kuzmina, A.M., Goreva, A.V., Shishatskaya, E.I., Hasirci, N., and Hasirci, V. In vitro and transdermal penetration of PHBV micro/nanoparticles. Journal of Materials Science: Materials in Medicine 25(6) (2014): 1471-1481.

[7] Li, S. and Malmstadt, N. Deformation and poration of lipid bilayer membranes by cationic nanoparticles. Soft Matter 9(20) (2013): 4969-4976.

[8] Sheng, R., Zhuang, X., Wang, Z., Cao, A., Lin, K., and Zhu, J.X.X. Cationic Nanoparticles Assembled from Natural-Based Steroid Lipid for Improved Intracellular Transport of siRNA and pDNA. Nanomaterials 6(4) (2016): 69.

[9] Czapar, A.E., et al. Tobacco Mosaic Virus Delivery of Phenanthriplatin for Cancer therapy. ACS Nano 10(4) (2016): 4119-4126.

[10] Li, M., Jiang, Y., Gong, T., Zhang, Z., and Sun, X. Intranasal Vaccination against HIV-1 with Adenoviral Vector-Based Nanocomplex Using Synthetic TLR-4 Agonist Peptide as Adjuvant. Molecular Pharmaceutics 13(3) (2016): 885-894.

[11] Kurrikoff, K., Gestin, M., and Langel, Ü. Recent in vivo advances in cell-penetrating peptide-assisted drug delivery. Expert Opinion on Drug Delivery 13(3) (2016): 373-387.

[12] Fischer, D., Li, Y., Ahlemeyer, B., Krieglstein, J., and Kissel, T. In vitro cytotoxicity testing of polycations: influence of polymer structure on cell viability and hemolysis. Biomaterials 24(7) (2003): 1121-1131.

[13] Merkel, O.M., et al. Polymer-related off-target effects in non-viral siRNA delivery. Biomaterials 32(9) (2011): 2388-2398.

[14] Arayachukeat, S., Palaga, T., and Wanichwecharungruang, S.P. Clusters of Carbon Nanospheres Derived from Graphene Oxide. ACS Applied Materials & Interfaces 4(12) (2012): 6808-6815.

[15] Arayachukiat, S., et al. Bringing Macromolecules into Cells and Evading Endosomes by Oxidized Carbon Nanoparticles. Nano Letters 15(5) (2015): 3370-3376.

[16] Rieker, T.P., Hindermann-Bischoff, M., and Ehrburger-Dolle, F. Small-Angle X-ray Scattering Study of the Morphology of Carbon Black Mass Fractal Aggregates in Polymeric Composites. Langmuir 16(13) (2000): 5588-5592.

[17] Li Volsi, G. Plasma Membrane as a Semipermeable Barrier. in Drug Delivery Across Physiological Barriers, pp. 41-63: Pan Stanford, 2016.

[18] McMahon, H.T. and Boucrot, E. Molecular mechanism and physiological functions of clathrin-mediated endocytosis. Nat Rev Mol Cell Biol 12(8) (2011): 517-533.

[19] Yang, N.J. and Hinner, M.J. Getting Across the Cell Membrane: An Overview for Small Molecules, Peptides, and Proteins. Methods in molecular biology (Clifton, N.J.) 1266 (2015): 29-53.

[20] Dupont, E., Prochiantz, A., and Joliot, A. Penetratin Story: An Overview. in Langel, Ü. (ed.)Cell-Penetrating Peptides: Methods and Protocols, pp. 29-37. New York, NY: Springer New York, 2015.

[21] Lönn, P. and Dowdy, S.F. Cationic PTD/CPP-mediated macromolecular delivery: charging into the cell. Expert Opinion on Drug Delivery 12(10) (2015): 1627-1636.

[22] Belting, M. and Wittrup, A. Developments in Macromolecular Drug Delivery. in Belting, M. (ed.)Macromolecular Drug Delivery: Methods and Protocols, pp. 1-10. Totowa, NJ: Humana Press, 2009.

[23] van den Berg, A. and Dowdy, S.F. Protein transduction domain delivery of therapeutic macromolecules. Current Opinion in Biotechnology 22(6) (2011): 888-893.

[24] Koren, E. and Torchilin, V.P. Cell-penetrating peptides: breaking through to the other side. Trends in Molecular Medicine 18(7) (2012): 385-393.

[25] Lundberg, M. and Johansson, M. Positively Charged DNA-Binding Proteins Cause Apparent Cell Membrane Translocation. Biochemical and Biophysical Research Communications 291(2) (2002): 367-371.

[26] Nakase, I., Tanaka, G., and Futaki, S. Cell-penetrating peptides (CPPs) as a vector for the delivery of siRNAs into cells. Molecular BioSystems 9(5) (2013): 855-861.

[27] Wadia, J.S., Stan, R.V., and Dowdy, S.F. Transducible TAT-HA fusogenic peptide enhances escape of TAT-fusion proteins after lipid raft macropinocytosis. Nat Med 10(3) (2004): 310-315.

[28] Cha, C., Shin, S.R., Annabi, N., Dokmeci, M.R., and Khademhosseini, A. Carbon-Based Nanomaterials: Multifunctional Materials for Biomedical Engineering. ACS Nano 7(4) (2013): 2891-2897.

[29] Bhattacharya, K., et al. Biological interactions of carbon-based nanomaterials: From coronation to degradation. Nanomedicine: Nanotechnology, Biology and Medicine 12(2): 333-351.

[30] Wang, Y., Li, Z., Hu, D., Lin, C.-T., Li, J., and Lin, Y. Aptamer/Graphene Oxide Nanocomplex for in Situ Molecular Probing in Living Cells. Journal of the American Chemical Society 132(27) (2010): 9274-9276.

[31] Feng, L., Zhang, S., and Liu, Z. Graphene based gene transfection. Nanoscale 3(3) (2011): 1252-1257.

[32] Shen, H., et al. PEGylated Graphene Oxide-Mediated Protein Delivery for Cell Function Regulation. ACS Applied Materials & Interfaces 4(11) (2012): 6317-6323.

[33] Seemork, J., et al. Penetration of Oxidized Carbon Nanospheres through Lipid Bilayer Membrane: Comparison to Graphene Oxide and Oxidized Carbon Nanotubes, and Effects of pH and Membrane Composition. ACS Applied Materials & Interfaces 8(36) (2016): 23549-23557.

[34] Pisetpackdeekul, P., et al. Proretinal nanoparticles: stability, release, efficacy, and irritation. International Journal of Nanomedicine 11 (2016): 3277-3286.

[35] OECD. Test No. 439: In Vitro Skin Irritation: Reconstructed Human Epidermis Test Method. OECD Publishing.

[36] Hjelm, R., Wampler, W., Gerspacher, M., and Worth, F. The structure of carbon black and its associations in elastomer composites: a study using neutron scattering. KAUTSCHUK UND GUMMI KUNSTSTOFFE 53(10) (2000): 592-595.

[37] Kim, K.-J. and White, J. Dispersion of Agglomerated Nanoparticles in Rubber Processing. in Polymer Nanocomposites Handbook: CRC Press, 2009.

[38] Sverre Myhra, J.C.R. Techniques and Methods for Nanoscale Analysis of Single Particles and Ensembles of Particles. in Characterization of Nanostructures, pp. 135-168: CRC Press, 2012.

[39] Li, J., et al. A review on phospholipids and their main applications in drug delivery systems. Asian Journal of Pharmaceutical Sciences 10(2) (2015): 81-98.

[40] Yuan, C., Furlong, J., Burgos, P., and Johnston, L.J. The Size of Lipid Rafts: An Atomic Force Microscopy Study of Ganglioside GM1 Domains in Sphingomyelin/DOPC/Cholesterol Membranes. Biophysical Journal 82(5) (2002): 2526-2535.

[41] Dodane, V. and Vilivalam, V.D. Pharmaceutical applications of chitosan. Pharmaceutical Science & Technology Today 1(6) (1998): 246-253.

[42] Didierjean, L., Tran, C., Sorg, O., and Saurat, J.H. Biological Activities of Topical Retinaldehyde. Dermatology 199(suppl 1)(Suppl. 1) (1999): 19-24.

VITA

Miss. Kittima Amornwachirabodee was born on April 23, 1987 in Bankok, Thailand. She received a Bachelor's Degree of Science in Chemistry from Chulalongkorn University in 2008. After that, she received a Master's degree in the Program of Chemistry, Faculty of Science, Chulalongkorn University. She has started Doctoral degree in the Program Chemistry, Faculty of Science, Chulalongkorn University under the supervision of Associate Professor Supason Wanichwecharungruang. After that, she has started Dual Doctoral degree between Chulalongkorn University and Japan Advance Institute Science and Technology (JAIST) in 2013. She has started Doctoral degree in school of Materials science, JAIST under the supervision of Professor Tatsuo Kaneko.

Her present address is 939/17 Klongjan, Bangkapi, Bangkok Thailand 10240. Tel. 099-396-3691